

GEOPHYSICS®

Comparison of the Inverse Scattering Series (ISS) Free-Surface Multiple-Elimination (FSME) algorithm, and the industry-standard SRME: Defining the circumstances where each method is the appropriate tool-box choice

Journal:	<i>Geophysics</i>
Manuscript ID	GEO-2018-0411.R1
Manuscript Type:	Technical Paper
Keywords:	algorithm, scattering, SRME (surface-related multiple elimination), multiples
Area of Expertise:	Seismic Migration, Seismic Modeling and Wave Propagation

SCHOLARONE™
Manuscripts

ABSTRACT

The Surface-Related Multiple Elimination (SRME) prediction followed by an adaptive subtraction has been (and will continue to be) the industry-standard to remove free-surface multiples. SRME is understood to provide an approximate predictor of the amplitude and phase of free-surface multiples. That recognition then places within the method itself an energy-minimization adaptive-subtraction step that seeks an indirect method to bridge the difference between the SRME prediction and the actual free-surface multiples. The criteria of energy-minimization is reasonable and often valid for isolated free-surface multiples that are not proximal with other events. However, for free-surface multiples that are proximal to other events, the criteria behind energy-minimization adaptive-subtraction can be invalid. When applied under those circumstances, the proximal primary often can be damaged. One way to reduce the dependence on the adaptive process is to obtain a more accurate free-surface-multiple prediction. The Inverse Scattering Series (ISS) Free-Surface Multiple Elimination (FSME) can predict free-surface multiples with accurate time and accurate amplitude for a multi-dimensional earth, without any subsurface information. Using 1D prestack examples, a quantitative comparison is performed between the predicted free-surface multiples by the ISS FSME, predicted free-surface multiples by the SRME and actual free-surface multiples. We point out the origin of their differences in the physics behind each method. The focus of this paper is to quantify the difference in the presence of interfering events with analytic data. The analysis confirms that the ISS FSME can predict free-surface multiples with accurate time and amplitude. The contribution of the SRME method has been recognized and it will continue to be an important toolbox option in the multiple-removal toolbox. The ISS FSME adds one option in the multiple-removal toolbox with a more accurate free-surface multiple prediction. It is called for and indicated

1
2
3
4 and appropriate choice for removing interfering free-surface multiples without damaging the
5
6 primaries
7
8
9
10
11
12
13
14
15
16
17
18
19
20
21
22
23
24
25
26
27
28
29
30
31
32
33
34
35
36
37
38
39
40
41
42
43
44
45
46
47
48
49
50
51
52
53
54
55
56
57
58
59
60

For Peer Review

INTRODUCTION

In the beginning of the paper, it is useful to remind ourselves of the definitions of seismic events based on their travel histories (Weglein et al., 2003). For instance, figure 1 shows different types of seismic events in marine seismic exploration. In marine seismic exploration, reference waves are *first* defined as waves that travel directly from source to receiver and waves that first travel up to the air-water boundary and then to the receiver. These two types of waves did not experience the subsurface. All other events have experienced the subsurface. *Then*, among the waves that did experience the subsurface, ghost events are defined as the seismic events that begin their propagation histories by traveling up from the source to the air-water boundary (source ghosts) or end their histories by traveling down from the air-water boundary to the receiver (receiver ghosts) or both (source-and-receiver ghosts). *After that*, events that begin their history going downward from the source and end their history upward at the receiver are divided into primary events and multiple events. Primary events are defined as the events that experience only one upward reflection during their propagation history, whereas multiple events are defined as the events that experience multiple reflections during their propagation history. Multiple events are further divided into free-surface multiples and internal multiples depending on the location of downward reflection between two consecutive upward reflections.

Multiples that have at least one downward reflection at the air-water (for offshore exploration) or air-land (for onshore exploration) surface are called free surface multiples, whereas multiples that have all of their downward reflections below the air-water or air-land surface are called internal multiples (Weglein et al., 1997). The order of a free-surface multiple is defined as the number of reflections it has experienced only at the air-water

1
2
3
4 or air-land surface. In contrast, the order of an internal multiple is defined by the total
5
6 number of downward reflections below the air-water or air-land surface. Notice that, these
7
8 definitions of different event types follow a sequence.
9

10
11 In principle, only primaries are called for to determine structure and to identify sub-
12
13 surface properties (Weglein, 2016, 2018). To obtain a data set containing of primaries, all
14
15 other events need to be predicted and removed. Hence, multiples, along with the refer-
16
17 ence waves, source ghosts, receiver ghosts and source-and-receiver ghosts, all need to be
18
19 predicted and removed from the seismic data in order to obtain the primary-only input to
20
21 imaging and inversion methods. There are two types of primaries and multiples: recorded
22
23 primaries and multiples, and unrecorded primaries and multiples. Recorded multiples can
24
25 be used to provide an approximate image of an unrecorded primary. Unrecorded multiples
26
27 must be removed in order to use a recorded multiple to find an approximate image of an
28
29 unrecorded primary. Currently in the petroleum industry, smooth velocity models are used
30
31 to locate structure and perform amplitude analysis. For a smooth velocity model, multiples
32
33 will always produce imaging artifacts. Therefore, multiples (both recorded and unrecorded)
34
35 need to be removed first from the reflection data before imaging primaries for processing
36
37 goals that seek to effectively locate and invert reflections. This paper will confine itself to
38
39 removing recorded multiples.
40
41
42
43
44
45

46 Both removing and using multiples are seeking the images of primaries: recorded pri-
47
48 maries and unrecorded primaries, respectively. As pointed out in Weglein (2018), the rela-
49
50 tionship between ‘removing multiples’ and ‘using multiples’ is not adversarial but comple-
51
52 mentary. This paper belongs to the study of the methods in ‘removing multiples’.
53
54

55 The methods for removing multiples have advanced and have become more effective.
56
57
58
59
60

1
2
3
4 However, the concomitant industry trend towards ever more complex exploration areas and
5
6 difficult plays has at times outpaced advances in multiple-attenuation capability. For exam-
7
8 ple, currently, the removal of multiples, especially those that are interfering with primaries,
9
10 for an unknown and complex multidimensional subsurface, remains a key open issue, and
11
12 high priority pressing challenge. We advocate a tool-box approach, in general, and seek
13
14 to understand the place and role that each method within the toolbox plays within the
15
16 spectrum of different capabilities and responses, and how to choose the method that's a
17
18 best match for the user's application and objective. We also advocate adding new options
19
20 to the toolbox to increase the collection of circumstances that can be addressed.
21
22
23
24

25 In this particular paper, we examine and compare two methods (i.e., the Inverse Scat-
26
27 tering Series Free-Surface Multiple Elimination (ISS FSME) (Carvalho et al., 1991; Weglein
28
29 et al., 1997, 2003) and the Surface-Related Multiple Elimination (SRME)) (Berkhout, 1985;
30
31 Verschuur, 1991; Verschuur et al., 1992) for the removal of *free-surface* multiples. We sug-
32
33 gest a guide to when each can be the appropriate choice within the free-surface-multiple-
34
35 removal toolbox. The SRME method has been widely used has become (and will remain)
36
37 the workhorse and industry-standard for removing free-surface multiples. Similarly, the ef-
38
39 fectiveness of the ISS FSME has been demonstrated in many complicated synthetic and field
40
41 data tests (e.g., Carvalho and Weglein (1994); Maston et al. (1999); Weglein and Dragoset
42
43 (2005); Zhang (2007); Ferreira (2011)).
44
45
46
47

48 These free-surface multiple removal methods share a property that both methods do not
49
50 require subsurface information. However, there are significant and well-documented differ-
51
52 ence between these two methods as discussed in Weglein, Matson and Berkhout (2000);
53
54 Weglein et al. (2000); Weglein and Dragoset (2005). For example, one difference is the
55
56 SRME method predicts the approximate amplitude and time of free-surface multiples. In
57
58
59
60

1
2
3
4 contrast, the ISS FSME method predicts free-surface multiples with both the accurate am-
5
6 plitude and accurate time. There are circumstances where that difference will be significant
7
8 and make a difference for removing free-surface multiples without damaging interfering or
9
10 proximal primaries.
11

12
13 Our aim and single objective is to use examples in 1D with analytic input data to provide
14
15 a quantitative analysis between two methods in terms of predicting free-surface multiples
16
17 and removing interfering free-surface multiples without damaging primaries. The outline
18
19 of the paper is as follows: we first describe the ISS free-surface multiple prediction and
20
21 SRME free-surface multiple prediction. We study the physics theory origin of the difference
22
23 between the ISS FSME and the SRME predictions. After that, we use 1D prestack examples
24
25 for a quantitative comparison of the free-surface multiple prediction between the ISS FSME
26
27 and SRME methods. In the end, we have discussion and conclusion.
28
29
30
31

32 33 34 **THE INVERSE SCATTERING SERIES (ISS) FREE-SURFACE** 35 36 **MULTIPLE ELIMINATION (FSME) ALGORITHM** 37 38

39 In this section, we describe the ISS FSME algorithm (Carvalho et al., 1991; Weglein et al.,
40
41 1997, 2003). We start by first describing the pre-processing steps before the ISS FSME and
42
43 then describing the ISS free-surface multiple prediction.
44
45

46 We use a 2D marine case as an example to illustrate the steps. Given the recorded
47
48 seismic data (see figure 1), $D(x_g, x_s, t)$ where x_g, x_s and t represent receiver and source
49
50 locations, and time, respectively. **(1)** The first step is to remove the reference waves. **(2)**
51
52 After the removal of reference waves, the second step is to remove source ghosts, receiver
53
54 ghosts and source-and-receiver ghosts.
55
56
57
58
59
60

(3) After the removal of reference waves and all ghosts (i.e., source ghosts, receiver ghosts and source-and-receiver ghosts), seismic data (represented by $D'_1(x_g, x_s, t)$) enters the ISS FSME to predict and remove free-surface multiples as follows:

- $D'_1(x_g, x_s, t)$ is first Fourier transformed over x_g, x_s, t (i.e., $D'_1(x_g, x_s, t) \rightarrow D'_1(k_g, k_s, \omega)$, see A-22 for Fourier transform convention).
- After Fourier transform, $D'_1(k_g, k_s, \omega)$ enters the ISS free-surface-multiple-prediction equations (i.e., equation 1) to predict free-surface multiples (represented by $D'_n(k_g, k_s, \omega)$, where $n = 2, 3, 4, \dots$) with both accurate time and accurate amplitude (in opposite polarity compared with actual free-surface multiples),

$$D'_n(k_g, k_s, \omega) = -\frac{1}{2\pi A(\omega)} \int dk e^{iq(z_g+z_s)} D'_1(k_g, k, \omega) (2iq) D'_{n-1}(k, k_s, \omega),$$

$$n = 2, 3, 4, \dots \quad (1)$$

The quantities $A(\omega)$, z_g and z_s in Equ. 1 are the source signature, receiver depth and source depth, respectively. $q = \sqrt{\frac{\omega^2}{c_0^2} - k^2}$.

- Then, these predicted free-surface multiples ($D'_n(k_g, k_s, \omega)$, where $n = 2, 3, 4, \dots$) are Inverse Fourier transformed to x_g, x_s and t , and added to the input data $D'_1(x_g, x_s, t)$ to obtain data without free-surface multiples, see equation 2.

$$D'(x_g, x_s, t) = D'_1(x_g, x_s, t) + D'_2(x_g, x_s, t) + D'_3(x_g, x_s, t) + \dots,$$

$$= \sum_{n=1}^{\infty} D'_n(x_g, x_s, t). \quad (2)$$

The output of the ISS FSME, $D'(x_g, x_s, t)$, represents the data without reference waves, without all ghosts, and without free-surface multiples.

It should be mentioned that the subsequent prediction terms in the series (equation 2), represented by D'_2, D'_3, \dots , provide predictions of free-surface multiples of different orders.

Specifically, each term in D'_n (where $n = 2, 3, 4, \dots$) when added to the earlier terms in the series (including the data D'_1) performs two functions: (1) it eliminates the n th order free-surface multiple. and (2) it alters all higher order free-surface multiples to be prepared for their removal by higher-order D'_j terms, where $j = n + 1, n + 2, \dots$.

The sum of these predictions ($D'_2 + D'_3 + \dots + D'_{n+1}$) will provide free-surface-multiple predictions with accurate time and accurate amplitude (in opposite polarity) for free-surface multiples up to n -th order (Weglein et al., 2003; Zhang and Shaw, 2010; Ma and Weglein, 2016).

The 2D SRME free-surface-multiple prediction, denoted by M , (Berkhout, 1985; Verschuur, 1991; Verschuur et al., 1992) is calculated by using seismic data without reference waves and without receiver-side ghosts, but retaining source-side ghosts, denoted by P , as follows,

$$M(x_g, x_s; \omega) = \int P(x_g, x; \omega) P(x, x_s; \omega) dx. \quad (3)$$

In the above equation 3, x_g, x_s, ω are receiver and source location and temporal frequency, respectively. To derive equation 3 one would have assumed that the data was generated by a vertically-separated dipole source in the water column with the reference waves removed and with source and receiver deghosted data (see details in Appendix B). Notice that, the monopole source itself together with its source ghost is assumed in the SRME prediction step to be a reasonable approximation to the dipole source (see figure B-1).

The physics theory difference between these two free-surface-multiple-prediction algorithms is studied in the Appendix A and Appendix B. In the next section, we focus on a quantitative comparison between the ISS and SRME free-surface multiple predictions.

A QUANTITATIVE COMPARISON BETWEEN THE ISS AND SRME FREE-SURFACE MULTIPLE PREDICTIONS

In this section, we aim to provide a quantitative comparison between the ISS free-surface multiple prediction and SRME free-surface multiple prediction.

From last section, we know the input data to the two free-surface multiple-prediction algorithms is different. For the ISS FSME the input is seismic data generated by a monopole source and without reference waves and without all ghosts (see figure 2, I), whereas for the SRME the input is seismic data generated by a dipole source and without reference waves and without all ghosts. However, in practice, since a data due to a vertically-separated dipole source is not realizable, the assumption within SRME is to approximate what a dipole source would produce by a monopole source and its source-side ghosts (see figure B-1 and figure 2, II (a)).

Following that, in the first set of comparisons (see the first bullet in figure 3), we provide different inputs to these two free-surface multiple-prediction algorithms. For ISS free-surface multiple-prediction algorithm, we use data due to a monopole source without reference waves and without all ghosts. For SRME free-surface multiple-prediction algorithm, we use data due to a monopole source without reference waves and without receiver-side ghosts (source-side ghosts are retained in the data).

In addition to the first set of comparisons, in practice, both source ghosts and receiver ghosts are removed before removing free-surface multiples for e.g., broad-band purpose. Hence, we carry out another set of comparisons with input data without reference waves and without all ghosts for both algorithms, with and without noise (see the second and third bullet in figure 3).

1
2
3
4 In the third set of comparisons, we input data generated by an absorptive medium and
5
6 without reference waves and without all ghosts (see the fourth bullet in figure 3). We
7
8 aim to confirm that for input data generated by an absorptive medium, both free-surface
9
10 multiple-prediction algorithms remain effective, i.e., the ISS predicts free-surface multiples
11
12 with both accurate amplitude and time, and the SRME predicts free-surface multiples
13
14 with both accurate amplitude and time, and the SRME predicts free-surface multiples with
15
16 approximate amplitude and time in the presence of absorptive medium.
17

18 19 **A first set of comparisons**

20
21
22
23 In this first set of comparisons, given their assumed input of these two free-surface multiples
24
25 algorithms, we provide a quantitative comparison of the predicted free-surface multiples by
26
27 the ISS and the SRME. In other words, for ISS free-surface multiple prediction, the input
28
29 data is without reference waves and without all ghosts; for SRME free-surface multiple
30
31 prediction, the input data is without reference waves and without receiver ghosts (the
32
33 source ghosts are retained in its input data).
34
35
36

37
38 Figure 4 shows the model with one horizontal reflector and a free-surface. Based on
39
40 this model, we use Cagniard-de Hoop (CdH) method (Cagniard (1939); de Hoop (1959)) to
41
42 generate the data. For a model with one horizontal reflector and a free-surface, CdH method
43
44 is able to obtain the analytical solutions of different events separately. This allows us to
45
46 (1) generate input data according to each algorithm's assumed input and (2) attribute any
47
48 difference in the comparison to the two prediction algorithms rather than the input analytic
49
50 data. Figures 5 and 6 show the input to the ISS and SRME free-surface multiple predictions,
51
52 respectively. Figures 7 and 8 show the prediction results from the ISS and SRME. Notice
53
54 that, for the ISS free-surface multiple prediction, we use equation 1 for $n = 2$. Figures
55
56
57
58
59
60

9 and 10 show the trace comparison at 500m offset between the the input data and free-surface multiple predictions from ISS and SRME, respectively. The result show that the ISS FSME predicts free-surface multiples with accurate time and accurate amplitude, whereas the SRME predicts free-surface multiples with approximate time and amplitude.

A second set of comparisons

Figure 11 shows the model we used to generate analytic input data in (k_x, ω) domain for a 1D subsurface. For example, a primary due to a horizontal reflector has an analytic form shown below (see e.g., Stolt and Weglein (1985)):

$$-R(k_x, \omega) \frac{e^{iq(2a-z_g-z_s)}}{2iq}, \quad (4)$$

where $R(k_x, \omega)$, a , z_g and z_s are plane wave reflection coefficient, depths of the reflector, receiver and source, respectively; $q = \sqrt{\frac{\omega^2}{c_0^2} - k_x^2}$, c_0 is the velocity above the reflector. For this model, the above expression for a primary can be extended to analytically generate other events separately. A Ricker wavelet with peak frequency at 30Hz is convolved with the analytic form to generate the data.

Notice that, in our example, (1) only three events (two primaries and one free-surface multiple) are generated, (2) the depths of the reflectors and velocities are chosen such that the second primary destructively interferes with the free-surface multiple. We examine two cases using input data with and without random noise. Notice that, the only difference between these two tests is the input data, input data for test 1 contains no noise whereas input data for test 2 contains random noise.

For test 1, Figures 12 to 16 show the synthetic input data, ISS free-surface multiple prediction, SRME free-surface multiple prediction, results after the ISS FSME and

1
2
3
4 SRME+adaptive, and the actual primary, respectively. Please notice that for the predic-
5
6 tions of free-surface multiples in figure 13 and figure 14, higher-order free-surface multiples
7
8 are also predicted. Please also note that the result from ISS FSME was obtained by di-
9
10 rectly subtracting the ISS prediction result from the data without an adaptive procedure,
11
12 whereas the result from SRME was obtained by combining the SRME free-surface multiple
13
14 prediction and the adaptive procedure.
15
16

17
18 Comparing the primary in the data (figure 17) with the multiple-removal result after
19
20 ISS FSME (figure 15), we find that, with the accurate multiple prediction, the ISS FSME
21
22 has surgically removed the free-surface multiple and recovered the primary.
23
24

25
26 Comparing the original data (figure 12) with the result after SRME + adaptive (figure
27
28 16), we notice, combining the approximate multiple prediction with the adaptive subtrac-
29
30 tion, the SRME can successfully remove the isolated multiple. The isolated free-surface
31
32 multiple in figure 12 is removed in figure 16. In figure 16 the arrows point to the removed
33
34 free-surface multiple. But the adaptive procedure can easily damage the primary which
35
36 interferes with the multiple (red circle in figure 16). It is worth mentioning that, we em-
37
38 ployed least-square (L2-norm) energy minimization adaptive subtraction, which is a current
39
40 standard practice in the industry, to remove the predicted free surface multiple event from
41
42 the data in figure 16.
43
44
45

46
47 Figures 18 to 22 provide trace plots to examine the results in detail at different offsets.
48
49 In these trace plots, red, blue and green lines represent actual data, ISS FSME multiple
50
51 prediction and SRME multiple prediction, respectively. From the offsets 100m, 500m, 1000m
52
53 and 1250m, where primary and multiple do not overlap, we can clearly see the ISS multiple
54
55 prediction matches the actual multiple in the data, whereas the SRME prediction shows a
56
57
58
59
60

1
2
3
4 disagreement.

5
6
7 Notice that, at offset 750m, the primary and multiple overlap. figure 23 shows the
8
9 comparison between the actual primary (blue line) with the multiple-removal result after
10
11 ISS FSME (red line) and the multiple-removal result after SRME+adaptive (green line) at
12
13 offset 750m. This figure shows the primary can be recovered by ISS FSME whereas the
14
15 SRME combined with the adaptive could damage the primary.
16
17

18
19 For test 2 in which the input data have random noise, figures 24 to 29 show the synthetic
20
21 input data, multiple prediction results from ISS FSME, SRME, results after the ISS FSME
22
23 and SRME+adaptive, and the actual primary, respectively. Similarly, figures 30 to 35
24
25 provide trace plots. Examining these comparisons, we can draw the similar conclusion as
26
27 in the case without noise.
28
29

30 31 32 **A third set of comparisons**

33
34
35 Weglein et al. (2003) showed the model-type independent properties of both ISS free-surface
36
37 multiple elimination algorithm and internal multiple attenuation algorithm. The meaning of
38
39 model-type independent is that the the removal of free-surface multiples is achievable with
40
41 precisely the same algorithm for an entire class of earth model types. The members of the
42
43 model type class include acoustic, elastic and certain anelastic media. Matson (1997) studied
44
45 and demonstrated the effectiveness of ISS elastic multiple removal from multicomponent
46
47 land and ocean bottom seismic data. Here, we provide a numerical example to demonstrate
48
49 and confirm the effectiveness of the ISS FSME algorithm for an absorptive medium.
50
51
52

53
54 The input data is generated based on model show in figure 11, with Q values 200,100,
55
56 and 100 for three layers from top to bottom. The analytic input data is generated using
57
58
59

1
2
3
4 the analytic forms of different events (see e.g., equation 4 for a primary) and a constant Q
5 model (known as frequency independent Q model), see Kolsky (1953). Figures 36, 37 and 38
6
7 show the input data, ISS free-surface multiple prediction and SRME free-surface multiple
8
9 prediction, respectively. Figures 39 and 40 show the result after the ISS FSME and SRME
10
11 + adaptive, respectively. Figures 42 to 46 show the trace comparison between the input
12
13 data, ISS free-surface multiple prediction and SRME free-surface multiple prediction at
14
15 offset 100m, 500m, 750m, 1000m, 1250m. Figure 47 show the trace comparison at offset
16
17 750m between the actual primary, result after the ISS FSME and result after the SRME
18
19 + adaptive. Examining the result of this test, we can conclude that, for data generated by
20
21 an acoustic medium that's absorptive, the same ISS FSME algorithm remains effective to
22
23 accurately predict the free-surface multiple and can surgically remove free-surface multiples
24
25 that interfere with primaries, without damaging primaries. We have numerically confirmed
26
27 that the ISS FSME algorithm remains effective with data from an absorptive medium. That
28
29 is consistent with the model type independent nature of the algorithm.
30
31
32
33
34
35

36 The ISS FSME is more computational costly than the SRME. The ISS free-surface
37
38 multiple prediction equation is in wavenumber-frequency domain, the obliquity factor in
39
40 it ($2iq$) precludes the transform from wavenumber-frequency domain to space-frequency
41
42 to obtain a convolutional equation (which is cheaper) as in SRME free-surface multiple
43
44 prediction.
45
46
47
48
49
50
51
52
53
54
55
56
57
58
59
60

DISCUSSION

Providing pre-requisites of the ISS FSME algorithm

The ISS FSME has the pre-requisites: source signature estimation, removal of reference waves, and source and receiver-side deghosting. Providing these pre-requisites is relatively mature for marine application. Advances in acquisition (e.g. over/under cable and dual-sensor towed streamer), have made the requirement of the following more effective methods realizable. Weglein and Secrest (1990), Osen et al. (1998), and Tan (1999) provide effective methods to estimate the source signature and radiation pattern using Green's theorem. For the removal of the reference waves, the distinct advantages (e.g., (1) no need for Fourier transforms over receivers and sources, and (2) can accommodate a horizontal or non-horizontal measurement surface) of applying Green's theorem method on marine data have been demonstrated by Weglein et al. (2002b); Zhang (2007); Mayhan and Weglein (2013). For deghosting, the industry widely used $P - V_z$ method (e.g., Amundsen (1993)) can be effective when the measurement surface is horizontal. The Green's theorem based deghosting method (Weglein et al. (2002a); Zhang (2007); Mayhan (2013)) has been extended to accommodate a depth-variable cable by the recent work of Wu and Weglein (2017), Zhang (2017) and Shen (2017). To provide the pre-requisites for on-land application, the recent work of Wu and Weglein (2014, 2015, 2016a,b) has contributed to extending off-shore Green's theorem preprocessing for wavelet estimation, reference waves (including ground roll) prediction and removal, and deghosting to the on-shore elastic case, in preparation for on-shore processing.

A new adaptive criteria that aligned with the algorithm itself

We have showed, given its pre-requisites, the ISS FSME will predict free-surface multiples with an accurate time and an accurate amplitude. These predicted multiples can be used to surgically remove free-surface multiples that interfere with primaries, without damaging the primaries. In practice, an adaptive step could still be needed. The energy-minimization criteria is viewed (by some thoughtful individuals) as the biggest impediment to effective multiple removal under complex circumstances. New adaptive criteria need to be developed. We are developing a new adaptive criteria derived as a property of the multiple removal algorithm. One candidate criteria is proposed in Weglein (2012).

CONCLUSION

We examined the origin of the missing obliquity factor in the SRME prediction step. We then used 1D prestack examples for a quantitative comparison of the free-surface-multiple prediction between the ISS FSME and SRME methods. The ISS FSME method provides a toolbox capability and option for a more accurate prediction of free-surface multiples. There are circumstances where this new and more effective capability might not be needed. For example, to remove isolated free-surface multiples, an approximated free-surface multiple prediction plus an adaptive subtraction by SRME method might be sufficient and suggested due to its less computational costs. However, there are many circumstances that this new capability is preferred. For example, (1) to remove a free-surface multiple that is interfering with a primary without damaging the primary, by providing a more accurate free-surface multiple prediction and relying less on the adaptive step. (2) And when it is unclear if a free-surface multiple is (or is not) interfering with a primary, the ISS FSME would be a

1
2
3
4
5
6
7
8
9
10
11
12
13
14
15
16
17
18
19
20
21
22
23
24
25
26
27
28
29
30
31
32
33
34
35
36
37
38
39
40
41
42
43
44
45
46
47
48
49
50
51
52
53
54
55
56
57
58
59
60

prudent choice. When this capability is needed, the ISS FSME method provides an option in the toolbox.

For Peer Review

APPENDIX A

THE ISS AND ITS SUBSERIES FOR FREE-SURFACE MULTIPLE ELIMINATION

Before the derivation of the Inverse Scattering Series (ISS) Free-Surface Multiple Elimination (FSME), we first provide (following Weglein et al. (2003)) a very brief introduction and background on the scattering series for solving seismic forward and inverse problems.

The seismic forward problem

The seismic forward modeling problem is to predict the wavefield in a medium when the medium properties that govern wave propagation in the medium and the source that generates the wavefield are prescribed. For example, for an acoustic, one parameter (variable velocity, constant density) medium, the single frequency wave equation for the pressure field due to a localized Dirac delta function source at \vec{r}_s

$$[\nabla^2 + k^2]G(\vec{r}, \vec{r}_s, \omega) = -\delta(\vec{r} - \vec{r}_s), \quad (\text{A-1})$$

where $k = \omega/c(\vec{r})$, ω is the temporal frequency and $c(\vec{r})$ is the velocity configuration. The wavefield $G(\vec{r}, \vec{r}_s, \omega)$ at \vec{r} due to source at \vec{r}_s can be modeled directly using e.g., a finite difference, finite element, Lattice Boltzman method given the medium properties $c(\vec{r})$ and the source function.

In scattering theory, the forward problem is derived differently. Scattering theory is a form of perturbation theory. That is, in scattering theory, the actual medium is separated into two parts, one part is called reference (the unperturbed) medium, the other part is called the perturbation (the difference between the actual medium and the reference medium). In

1
2
3
4 general, we can express the differential equations governing wave propagation in the actual
5
6 medium and reference medium as

$$7 \quad LG = -\delta(\vec{r} - \vec{r}_s), \quad (\text{A-2})$$

11 and

$$12 \quad L_0G_0 = -\delta(\vec{r} - \vec{r}_s), \quad (\text{A-3})$$

13
14
15 respectively. In the acoustic (variable velocity, constant density) model of equation A-1,
16
17 $L = \nabla^2 + k^2$ where $k = \omega/c(\vec{r})$. L, L_0 here are general differential operators in the actual and
18
19 reference medium, respectively. G, G_0 are the actual and reference wavefields, respectively.
20
21 δ is a Dirac delta source function, and \vec{r}, \vec{r}_s are the receiver and source locations, respectively.
22
23 The perturbation differential operator is defined as $V \equiv L - L_0$. Notice that the differential
24
25 operators L and L_0 contain the properties in the actual and the reference media that govern
26
27 wave propagation in those medium, respectively. Different Earth model-types are described
28
29 by different forms of operators L and L_0 . These operators contain the (spatially variant)
30
31 parameters of the specific earth model type (e.g., acoustic, elastic, anisotropic and anelastic).
32
33 For example, for an acoustic, variable velocity constant density model type, $L = \nabla^2 + k^2$,
34
35 where $k = \omega/c(\vec{r})$ as illustrated in equation A-1. $L_0 = \nabla^2 + k_0^2$, where $k_0 = \omega/c_0(\vec{r})$ as in
36
37 $[\nabla^2 + k_0^2]G_0(\vec{r}, \vec{r}_s, \omega) = -\delta(\vec{r} - \vec{r}_s)$.

38
39 We can express the actual medium differential operator L in terms of a reference medium
40
41 differential operator L_0 and a perturbation operator V as $L = L_0 + V$. The perturbation
42
43 operator is defined as $V = L - L_0$. Thus, equation A-2 can be written as

$$44 \quad (L_0 + V)G = -\delta, \quad (\text{A-4})$$

Rearranging the above expression as follows,

$$L_0G = -\delta - VG,$$

$$G = -L_0^{-1}\delta - L_0^{-1}VG \quad (\text{A-5})$$

Now substituting $\delta = -L_0G_0$ (equation A-3) and considering $L_0^{-1} = -G_0$, we have,

$$G = L_0^{-1}L_0G_0 - L_0^{-1}VG,$$

$$G = G_0 + G_0VG. \quad (\text{A-6})$$

The last equation A-6 is called the Lippmann-Schwinger equation (e.g., Taylor, 1972).

The Lippmann-Schwinger equation is an operator relationship between G (the wavefield in the actual medium), G_0 (the wavefield in the reference medium) and V (the perturbation). G appears on both sides of equation A-6. To solve A-6 for G we can treat $G = G_0$ (the first term on the right hand side of A-6) as a first approximation for G . Then substituting $G = G_0$ on the right hand side of A-6, we find an approximation for G as $G_0 + G_0VG_0$, and then once again substitute this expression for G on the right hand side of A-6 we find an updated approximation for G as

$$G_0 + G_0VG_0 + G_0VG_0VG_0. \quad (\text{A-7})$$

Then, continuing this successive substitution process for G on the right hand side of A-6, we find,

$$G = G_0 + G_0VG_0 + G_0VG_0VG_0 + G_0VG_0VG_0VG_0 + \dots \quad (\text{A-8})$$

The difference between the actual wavefield G and reference wavefield G_0 is defined as scattered wavefield, $\psi_s = G - G_0$.

The seismic *forward* problem is solved in scattering theory by equation A-8, i.e., given the reference wavefield G_0 and perturbation V (the right hand side of A-8), equation A-8

can be used as a forward modeling tool to obtain the actual wavefield G (the left hand of A-8). The recorded seismic data corresponds to the wavefield evaluated on the measurement surface.

The seismic inverse problem

The seismic *inverse* problem is to solve for the medium properties L in terms of measured wavefield and the source.

The seismic inverse problem is solved in scattering theory by first solving for V . Then V is added to the reference medium operator L_0 to obtain the actual medium operator L . To derive the inverse scattering method to solve for V , let's first examine the forward series A-8. We note that equation A-8 has the form of a generalized geometric series (Weglein, 2017)

$$G - G_0 = S = ar + ar^2 + ar^3 + \dots = \frac{ar}{1 - r}, \quad (\text{A-9})$$

for $|r| < 1$, where we have identified in our ??? analog $a = G_0$ and $r = VG_0$. If we identify $S_1 = ar, S_2 = ar^2, \dots$, as the portion of S linear in r , quadratic in r , etc, then, equation A-9 becomes

$$S = S_1 + S_2 + S_3 + \dots = \frac{ar}{1 - r}. \quad (\text{A-10})$$

Solving A-10 for r , in terms of S/a produces an inverse geometric series

$$r = \frac{S/a}{1 + S/a} = S/a - (S/a)^2 + (S/a)^3 + \dots, = r_1 + r_2 + r_3 + \dots, \quad (\text{A-11})$$

when $|S/a| < 1$, where r_n is the portion of r that is n th order in S/a .

For the seismic inverse problem, we associate S with the recorded values of the scattered wavefield $S = (\psi_s)_{ms} = (G - G_0)_{ms}$, and the forward series follow from treating the forward

1
2
3
4 solution as S in terms of V , and the inverse series as V in terms of S . The inverse series is
5
6 the analog of equation A-11, where r_1, r_2, \dots are replaced with V_1, V_2, \dots :
7
8

$$9 \quad V = V_1 + V_2 + V_3 + \dots, \quad (\text{A-12})$$

10
11 where V_n is the portion of V that is n th order in the data, D . Substituting equation A-12
12
13 into equation A-8 and evaluating both sides of equation A-8 on the measurement surface,
14
15 and setting terms of equal order in the data equal, produces the following set of equations
16
17
18

$$19 \quad (\psi_s)_{ms} = (G_0 V_1 G_0)_{ms}, \quad (\text{A-13})$$

$$20 \quad 0 = (G_0 V_2 G_0)_{ms} + (G_0 V_1 G_0 V_1 G_0)_{ms}, \quad (\text{A-14})$$

$$21 \quad 0 = (G_0 V_3 G_0)_{ms} + (G_0 V_2 G_0 V_1 G_0)_{ms} + (G_0 V_1 G_0 V_2 G_0)_{ms} + (G_0 V_1 G_0 V_1 G_0 V_1 G_0)_{ms}, \quad (\text{A-15})$$

$$22 \quad 0 = (G_0 V_n G_0)_{ms} + (G_0 V_1 G_0 V_{n-1} G_0)_{ms} + \dots + (G_0 V_1 G_0 V_1 G_0 V_1 \dots G_0 V_1 G_0)_{ms}. \quad (\text{A-16})$$

23
24
25
26
27
28
29
30
31
32 V_1 can be solved in equation A-13 using the measured scattered wavefield $(\psi_s)_{ms}$ and the
33
34 reference wavefield G_0 . Then, substitute V_1 into equation A-14, solve for V_2 as in equation
35
36 A-13. In this manner, we can compute any V_n only using the measured scattered wavefield
37
38 $(\psi_s)_{ms}$ and the reference wavefield G_0 . Hence $V = \sum_{n=1}^{\infty} V_n$ is an explicit direct inversion
39
40 solution, and doesn't require any subsurface information. The inverse step in A-13 - A-16
41
42 for V_1, V_2, V_3, \dots involves inverting the same unchanged operator G_0 and when the reference
43
44 medium is homogeneous that matrix inverse is analytic (Weglein et al., 2003).
45
46
47

48 The inverse scattering series methods were first developed by Moses (1956), Prosser
49
50 (1969) and Razavy (1975). Weglein et al. (1981) and Stolt and Jacobs (1980) applied
51
52 the inverse scattering series methods to extract multidimensional earth information from
53
54 seismic data. Carvalho (1992) performed empirical tests of the ISS method for a normal
55
56 incident plane wave on a 1D acoustic medium. The result indicated the full series only
57
58
59
60

1
2
3
4 convergences when the difference between the actual Earth's acoustic velocity and reference
5
6 velocity (water velocity) is less than 11%. In response, the idea of isolated task-specific
7
8 subseries was developed: (1) free-surface multiple elimination; (2) internal multiple at-
9
10 tenuation/elimination; (3) Q compensation without knowing or estimating Q; (4) depth
11
12 imaging; and (5) inversion (parameter estimation). The identification of terms in the ISS
13
14 to be included in a given task-specific subseries used several different types of analysis with
15
16 testing of new concepts to evaluate, refine and develop embryonic thinking largely based on
17
18 forward series processes and analogues and physical intuition (Weglein et al., 2003). For ex-
19
20 ample, for free-surface multiples, understanding how the forward scattering series produces
21
22 a free-surface multiple event provides a "hint" where the inverse process might be located.
23
24 That "hint", due to a symmetry between event creation and event removal, turns out to be
25
26 useful. For internal multiples location of terms that perform attenuation and elimination is
27
28 described in (Weglein et al., 2003) page R55-R62. For the purpose of this paper, it is useful
29
30 to review the thinking behind locating the ISS subseries for removing free-surface multiples.
31
32
33
34
35

36 G_0^{fs} corresponds to a wave due to a Dirac delta point source in the water column
37
38 that propagates up and reflects off the free-surface and has a field point below the free-
39
40 surface. In the absence of a free surface, a forward series equation (A-8) describing the
41
42 data is constructed from the direct propagating Green's function, G_0^d , and the perturbation
43
44 operator, V .
45
46
47

48 With the free surface present, the forward series is constructed from $G_0 = G_0^d + G_0^{fs}$ and
49
50 the same perturbation operator, V . Hence, G_0^{fs} is the sole difference between the forward
51
52 series with and without the free surface; therefore G_0^{fs} is responsible for generating those
53
54 events that owe their existence to the presence of the free surface, i.e., ghosts and free-
55
56 surface multiples. In the inverse series, equations (A-13) to (A-16), it is reasonable to infer
57
58
59
60

that G_0^{fs} will be responsible for all the extra tasks that inversion needs to perform when starting with data containing ghosts and free-surface multiples rather than data without those events. Those extra inverse tasks include deghosting and the removal of free-surface multiples.

The inverse series expansions, equations (A-13) to (A-16), consist of terms $(G_0 V_n G_0)_m$ with $G_0 = G_0^d + G_0^{fs}$. Source and receiver deghosting is realized by removing the two outside $G_0 = G_0^d + G_0^{fs}$ functions and replacing them with G_0^d .

Data is considered the measured values of scattered wavefield, equation A-13. The source and receiver deghosted data (represented by \tilde{D}), is related to V_1 as $\tilde{D} = (G_0^d V_1 G_0^d)_m$. After the deghosting operation, the objective is to remove the free-surface multiples from the deghosted data, \tilde{D} .

The terms in the inverse series expansions, (A-13) to (A-16), replacing D with input \tilde{D} , contain both G_0^d and G_0^{fs} between the operators V_i . The outer G_0^d 's (rather than $G_0 = G_0^d + G_0^{fs}$) indicate that the data have been source and receiver deghosted. The inner G_0^d and G_0^{fs} are where the four inversion tasks (internal multiple removal, depth imaging, Q compensation without knowing or estimating Q, inversion/parameter estimation) reside. If we consider the inverse scattering series and $G_0 = G_0^d + G_0^{fs}$, and if we assume that the data has been source and receiver deghosted (i.e., G_0^d replaces $(G_0^{fs} + G_0^d)$ on the outside contributions), then the terms in the series are of three types:

$$Type1 : \left(G_0^d V_i G_0^{fs} V_j G_0^{fs} V_k G_0^d \right)_{ms}$$

$$Type2 : \left(G_0^d V_i G_0^{fs} V_j G_0^d V_k G_0^d \right)_{ms}$$

$$Type3 : \left(G_0^d V_i G_0^d V_j G_0^d V_k G_0^d \right)_{ms} .$$

We interpret these types of terms from a task isolation point of view. Type 1 terms have

1
2
3
4 only G_0^{fs} between two V_i, V_j contributions; these terms when added to \tilde{D} remove free-surface
5
6 multiples and perform no other task. Type 2 terms have both G_0^d and G_0^{fs} between two V_i, V_j
7
8 contributions; these terms perform free-surface multiple removal *plus* a task associated with
9
10 G_0^d . Type 3 have only G_0^d between two V_i, V_j contributions; these terms do not remove any
11
12 free-surface multiples. The idea behind task separated subseries is two fold: 1) isolate the
13
14 terms in the overall series that perform a given task *as if no other tasks exist* (e.g., Type 1
15
16 above) and 2) not to return to the original inverse series with its coupled tasks involving
17
18 G_0^{fs} and G_0^d , but rather restart the problem with an input data free of free-surface multiples,
19
20 D' .
21
22
23
24

25 With the idea of task separated subseries, the subseries for removing free-surface mul-
26
27 tiples resides in Type 1 terms. Collecting all Type 1 terms, we have
28
29

$$30 \quad D'_1 \equiv \tilde{D} = (G_0^d V_1 G_0^d)_{ms}, \quad (\text{A-17})$$

$$31 \quad D'_2 = (G_0^d V_2 G_0^d)_m = -(G_0^d V_1 G_0^{fs} V_1 G_0^d)_{ms}. \quad (\text{A-18})$$

$$32 \quad D'_3 = - (G_0^d V_1 G_0^{fs} V_1 G_0^{fs} V_1 G_0^d)_{ms}$$

$$33 \quad - (G_0^d V_2 G_0^{fs} V_1 G_0^d)_{ms}$$

$$34 \quad - (G_0^d V_1 G_0^{fs} V_2 G_0^d)_{ms} \quad (\text{A-19})$$

35
36
37
38
39
40
41
42
43 ...

44
45
46 $D'_1 \equiv \tilde{D}$ is the first term; it is the seismic data after the removal of direct wave and source
47
48 and receiver deghosting.
49

50
51 D'_3 can be simplified as (see e.g., Weglein et al. (2003))

$$52 \quad D'_3 = (D_0^d V_1 G_0^{fs} V_1 G_0^{fs} V_1 G_0^d)_{ms}. \quad (\text{A-20})$$

Equation A-17 can be expressed as follows,

$$D'_1(x_g, z_g, x_s, z_s, \omega) = \int dx_1 dz_1 dx_2 dz_2 G_0^d(x_g, z_g, x_1, z_1, \omega) V_1(x_1, z_1, x_2, z_2, \omega) G_0^d(x_2, z_2, x_s, z_s, \omega). \quad (\text{A-21})$$

Following the Fourier transform convention defined in e.g., Clayton and Stolt (1981); We-
glein et al. (2003),

$$D(k_g, k_s, \omega) = \int \int \int D(x_g, x_s, t) e^{ik_s x_s - ik_g x_g + i\omega t} dt dx_g dx_s, \quad (\text{A-22})$$

Fourier transforming over x_g, x_s on both sides of equation A-21,

$$D'_1(k_g, z_g, k_s, z_s, \omega) = \int dx_1 dz_1 dx_2 dz_2 G_0^d(k_g, z_g, x_1, z_1, \omega) V_1(x_1, z_1, x_2, z_2, \omega) G_0^d(x_2, z_2, k_s, z_s, \omega). \quad (\text{A-23})$$

$G_0^d(k_g, z_g, x_1, z_1, \omega)$ and $G_0^d(x_2, z_2, k_s, z_s, \omega)$ are (see e.g., Clayton and Stolt (1981))

$$G_0^d(k_g, z_g, x_1, z_1, \omega) = -\frac{e^{-i(k_g x_1 - q_g |z_1 - z_g|)}}{2iq_g} = -\frac{e^{-i(k_g x_1 - q_g (z_1 - z_g))}}{2iq_g}, \quad (\text{A-24})$$

and

$$G_0^d(x_2, z_2, k_s, z_s, \omega) = -\frac{e^{i(k_s x_2 + q_s |z_2 - z_s|)}}{2iq_s} = -\frac{e^{i(k_s x_2 + q_s (z_2 - z_s))}}{2iq_s}, \quad (\text{A-25})$$

Respectively. Notice that, in equations A-24 and A-25, we have assumed $z_1 > z_g$ and $z_2 > z_s$ to remove the absolute value ($|z_1 - z_g| \rightarrow (z_1 - z_g)$, $|z_2 - z_s| \rightarrow (z_2 - z_s)$) in the Green's functions. That assumption corresponds to the assumption that the perturbation $V_1(x_1, z_1, x_2, z_2)$ is *below* the source z_s and receiver depth z_g (i.e., measurement surface). The positive direction for z is pointing downward, hence, perturbation below the measurement surface means $z_1 > z_g$ and $z_2 > z_s$.

Substituting equations A-24 and A-25 into equation A-23, we have

$$\begin{aligned} D'_1(k_g, z_g, k_s, z_s, \omega) &= \int dx_1 dz_1 dx_2 dz_2 \frac{e^{-i(k_g x_1 - q_g (z_1 - z_g))}}{2iq_g} V_1(x_1, z_1, x_2, z_2, \omega) \frac{e^{i(k_s x_2 + q_s (z_2 - z_s))}}{2iq_s} \\ &= \frac{e^{-iq_g z_g} e^{-iq_s z_s}}{2iq_g 2iq_s} V_1(k_g, q_g, k_s, q_s, \omega), \end{aligned} \quad (\text{A-26})$$

where we have recognize the integrals over x_1, z_1, x_2, z_2 as Fourier transforms.

Similarly, in Equation A-18,

$$D'_2(x_g, z_g, x_s, z_s, \omega) = \left(G_0^d(x_g, z_g, x_1, z_1) V_2(x_1, z_1, x_2, z_2, \omega) G_0^d(x_2, z_2, x_s, z_s, \omega) \right)_{ms}$$

can be expressed as

$$D'_2(k_g, z_g, k_s, z_s, \omega) = \frac{e^{-iq_g z_g} e^{-iq_s z_s}}{2iq_g 2iq_s} V_2(k_g, q_g, k_s, q_s, \omega). \quad (\text{A-27})$$

And for

$$\begin{aligned} & \left(G_0^d(x_g, z_g, x_1, z_1, \omega) V_2(x_1, z_1, x_2, z_2, \omega) G_0^d(x_2, z_2, x_s, z_s, \omega) \right)_{ms} = \\ & - \left(G_0^d(x_g, z_g, x_1, z_1, \omega) V_1(x_1, z_1, x_2, z_2, \omega) G_0^{fs}(x_2, z_2, x_3, z_3, \omega) V_1(x_3, z_3, x_4, z_4, \omega) \right. \\ & \left. \times G_0^d(x_4, z_4, x_s, z_s, \omega) \right)_{ms}, \end{aligned} \quad (\text{A-28})$$

the left hand side can be expressed as

$$LHS = \frac{e^{-iq_g z_g} e^{-iq_s z_s}}{2iq_g 2iq_s} V_2(k_g, q_g, k_s, q_s, \omega). \quad (\text{A-29})$$

To solve for the right hand side of equation A-28, we have $G_0^d(k_g, z_g, x_1, z_1, \omega)$ and $G_0^d(x_2, z_2, k_s, z_s, \omega)$ expressed in equations A-24, A-25, respectively. $G_0^{fs}(x_2, z_2, x_3, z_3, \omega)$ can be expressed as follows (see figure A-1),

$$G_0^{fs}(x_2, z_2, x_3, z_3, \omega) = \frac{1}{2\pi} \int dk \frac{e^{ik(x_2-x_3)} e^{iq(z_2+z_3)}}{2iq}, \quad (\text{A-30})$$

Notice that, we have assumed the free-surface is at depth $z = 0$ in this expression. The right hand side now can be expressed as follows,

$$\begin{aligned} RHS &= -G_0^d V_1 G_0^{fs} V_1 G_0^d = - \int dx_1 dz_1 dx_2 dz_2 dx_3 dz_3 dx_4 dz_4 \frac{e^{-i(k_g x_1 - q_g(z_1 - z_g))}}{2iq_g} \\ & \times V_1(x_1, z_1, x_2, z_2, \omega) \frac{1}{2\pi} \int dk \frac{e^{ik(x_2-x_3)} e^{iq(z_2+z_3)}}{2iq} V_1(x_3, z_3, x_4, z_4, \omega) \frac{e^{i(k_s x_4 + q_s(z_4 - z_s))}}{2iq_s} \\ & = - \frac{e^{-iq_g z_g} e^{-iq_s z_s}}{2iq_g 2iq_s} \frac{1}{2\pi} \int dk V_1(k_g, q_g, k, q, \omega) \frac{1}{2iq} V_1(k, q, k_s, q_s, \omega). \end{aligned} \quad (\text{A-31})$$

Canceling common factors on both sides (equations A-29 and A-31), we have

$$V_2(k_g, k_s, \omega) = -\frac{1}{2\pi} \int dk V_1(k_g, k, \omega) \frac{1}{2iq} V_1(k, k_s, \omega). \quad (\text{A-32})$$

Substituting V_1 with D'_1 using equation A-26 and V_2 with D'_2 using equation A-27, we obtain the second term D'_2 as follows,

$$D'_2(k_g, k_s, \omega) = -\frac{1}{2\pi} \int dk D_1(k_g, k, \omega) (2iq) e^{iq(z_g+z_s)} D_1(k, k_s, \omega). \quad (\text{A-33})$$

Next, we show one example from Zhang (2007) to demonstrate that the ISS free-surface multiple-prediction algorithm predicts free-surface multiples with accurate time and amplitude.

Figure A-2 shows the model used to generate input data. The generated data contain the reference waves (yellow line), source and receiver ghosts (dashed blue line), free-surface multiples (black line), and primaries (red line). This data is first pre-processed by Green's theorem to remove reference waves, source and receiver ghosts, then, the pre-processed data (contains only primaries and free-surface multiples, see solid line in figure A-3) enter the ISS FSME algorithm. The result after the ISS FSME is shown in figure A-3 using dashed line. Notice that, the result after the ISS FSME is obtained by $D'_2 + D'_1$. When D'_2 is added to D'_1 , two things happen, the first-order free-surface multiple is eliminated, all higher-order free-surface multiples are altered, and prepared for their removal by D'_3, D'_4 , etc.

APPENDIX B

COMPARING THE ISS FSME WITH SRME

In appendix A, we have provided a brief derivation of the ISS FSME algorithm. The ISS FSME inputs seismic data that is generated by monopole sources (or source arrays) and that

has the reference waves and source ghosts, receiver ghosts and source-and-receiver ghosts removed. This algorithm predicts the exact time and exact amplitude of all free-surface multiples at all offsets. That provides a good starting point and opportunity to understand under what set of approximations we can derive the SRME prediction with approximate prediction of the amplitude and phase of the free-surface multiples. That then locates and identifies the origin of the missing physics in the SRME prediction. It turns out that the SRME prediction corresponds to a data with the reference waves removed and with source and receiver deghosted data, but where the source consists of a vertically separately dipole source in the water column. The vertically-separated dipole source is defined as the limit of two vertically separately (of opposite sign) Dirac delta sources as the distance between them approaches zero and the source amplitude goes to infinity, in such a way that the product of source amplitude and the distance between them remains constant. Since a data due to a vertically dipole source is not realizable in practice, the idea within SRME is to somehow approximate what a dipole source would produce by keeping the source side ghost (see figure B-1). That substitution is the origin of the missing or erroneous physics and results in an approximate prediction of both amplitude and phase of the free-surface multiples. To put a light on that we examine the consequence of that substitution on the exact ISS FSME prediction in Appendix B.

Follow the SRME prescription to input the data with only direct wave and receiver-side ghosts removed (i.e., without source-side deghosting), in this case, equations A-17 to A-18 become

$$D_1'' = \left(G_0^d V_1 \left(G_0^d + G_0^{fs} \right) \right)_{ms}, \quad (\text{B-1})$$

$$D_2'' = \left(G_0^d V_2 \left(G_0^d + G_0^{fs} \right) \right)_{ms} = - \left(G_0^d V_1 G_0^{fs} V_1 \left(G_0^d + G_0^{fs} \right) \right)_{ms}. \quad (\text{B-2})$$

With

$$G_0^{fs}(x_2, z_2, k_s, z_s, \omega) = \frac{e^{i(k_s x_2 + q_s(z_2 + z_s))}}{2iq_s},$$

Equation B-1 now becomes,

$$D_1''(k_g, z_g, k_s, z_s, \omega) = \frac{e^{-iq_g z_g} (e^{-iq_s z_s} - e^{iq_s z_s})}{2iq_g 2iq_s} V_1(k_g, q_g, k_s, q_s, \omega) \quad (\text{B-3})$$

The left part of Equation B-2 becomes,

$$D_2''(k_g, z_g, k_s, z_s, \omega) = \frac{e^{-iq_g z_g} (e^{-iq_s z_s} - e^{iq_s z_s})}{2iq_g 2iq_s} V_2(k_g, q_g, k_s, q_s, \omega) \quad (\text{B-4})$$

The right part of equation B-2 becomes,

$$-\frac{e^{-iq_g z_g} (e^{-iq_s z_s} - e^{iq_s z_s})}{2iq_g 2iq_s} \frac{1}{2\pi} \int dk V_1(k_g, q_g, k, q, \omega) \frac{1}{2iq} V_1(k, q, k_s, q_s, \omega) \quad (\text{B-5})$$

We have,

$$V_2(k_g, k_s, \omega) = -\frac{1}{2\pi} \int dk V_1(k_g, k, \omega) \frac{1}{2iq} V_1(k, k_s, \omega) \quad (\text{B-6})$$

Now, substituting V_1, V_2 with D_1'', D_2'' in equations B-3 and B-4, respectively, we have

$$D_2''(k_g, z_g, k_s, z_s, \omega) = \frac{1}{2\pi} \int dk D_1''(k_g, z_g, k, z_s, \omega) \frac{2iqe^{iqz_g}}{(e^{iqz_s} - e^{-iqz_s})} D_1''(k, z_g, k_s, z_s, \omega). \quad (\text{B-7})$$

Let's take a look at the factor $(e^{iqz_s} - e^{-iqz_s})$ in the denominator. For a source that is close to the free-surface (which means z_s is small, since the free-surface is assumed to be at depth $z = 0$ in this case), the factor $(e^{iqz_s} - e^{-iqz_s})$ can be approximated by

$$e^{iqz_s} - e^{-iqz_s} \approx iqe^{-iqz_s} 2z_s.$$

Under this approximation, equation B-7 becomes

$$\begin{aligned} D_2''(k_g, z_g, k_s, z_s, \omega) &= \frac{1}{2\pi} \int dk D_1''(k_g, z_g, k, z_s, \omega) \frac{2iqe^{iqz_g}}{(e^{iqz_s} - e^{-iqz_s})} D_1''(k, z_g, k_s, z_s, \omega) \\ &\approx \frac{1}{2\pi} \int dk D_1''(k_g, z_g, k, z_s, \omega) \left(e^{iq(z_g + z_s)} \right) D_1''(k, z_g, k_s, z_s, \omega) \frac{1}{z_s} \end{aligned} \quad (\text{B-8})$$

Now, if receiver in the actual experiment is close to the free-surface (z_g is small), then equation B-8 will be proportional to

$$\frac{1}{2\pi} \int dk D_1''(k_g, z_g, k, z_s, \omega) D_1''(k, z_g, k_s, z_s, \omega). \quad (\text{B-9})$$

Inverse Fourier transform on k_g and k_s , we have

$$\frac{1}{2\pi} \int dk D_1''(x_g, k, \omega) D_1''(k, x_s; \omega).$$

Expressing $D_1''(x_g, k, \omega)$ and $D_1''(k, x_s; \omega)$ using their Fourier Transforms,

$$\frac{1}{2\pi} \int dk \int dx' D_1''(x_g, x'; \omega) e^{ikx'} \int dx'' D_1''(x'', x_s; \omega) e^{-ikx''}.$$

Rearrange the above equation,

$$\frac{1}{2\pi} \int dx' \int dx'' D_1''(x_g, x'; \omega) D_1''(x'', x_s; \omega) \int dk e^{ik(x' - x'')}.$$

We have

$$\begin{aligned} & \frac{1}{2\pi} \int dx' \int dx'' D_1''(x_g, x'; \omega) D_1''(x'', x_s; \omega) \int dk e^{ik(x' - x'')} \\ &= \frac{1}{2\pi} \int dx' \int dx'' D_1''(x_g, x'; \omega) D_1''(x'', x_s; \omega) \left(2\pi \delta(x' - x'') \right) \\ &= \int dx D_1''(x_g, x; \omega) D_1''(x, x_s; \omega). \end{aligned} \quad (\text{B-10})$$

We obtain the convolutional SRME free-surface-multiple-prediction equation. Hence, the industry standard free-surface algorithm, SRME, can be derived as an approximation to the ISS FSME algorithm. The ISS FSME predicts the exact time and amplitude of all free-surface multiples of different orders at all offsets. SRME predicts the approximate amplitude and phase of free surface multiples at all offsets.

REFERENCES

- Amundsen, L., 1993, Wavenumber-based filtering of marine point-source data: *Geophysics*, **58**, 1335–1348.
- Berkhout, A. J., 1985, *Seismic migration: Theoretical aspects*: Elsevier Publishing Co.
- Cagniard, L., 1939, *Reflexion et refraction des ondes sismiques progressive*: Gauthier-Villar.
- Carvalho, P. M., and Weglein, A. B., 1994, Wavelet estimation for surface multiple attenuation using a simulated annealing algorithm: *SEG Technical Program Expanded Abstracts*.
- Carvalho, P. M., Weglein, A. B., and Stolt, R. H., 1991, Examples of a nonlinear inversion method based on the T-matrix of scattering theory: Application to multiple suppression: *SEG Expanded Abstracts*, pages 1319–1322.
- Carvalho, P. M., 1992, Free-surface multiple reflection elimination method based on nonlinear inversion of seismic data: Ph.D. thesis, Universidade Federal da Bahia.
- Clayton, R. W., and Stolt, R. H., 1981, A Born-WKBJ inversion method for acoustic reflection data: *Geophysics*, **46**, no. 11, 1559–1567.
- de Hoop, A. T., 1959, The surface line source problem: *Appl. Sci. Res. B.*, **8**, 349–356.
- Ferreira, A., 2011, Internal multiple removal in offshore brazil seismic data using the inverse scattering series: Ph.D. thesis, University of Houston.
- Kolsky, H., 1953, The propagation of stress waves in viscoelastic solids: *Philosophical Magazine*, **1**, no. 8, 693–710.

- 1
2
3
4 Ma, C., and Weglein, A., 2016, Examining the interdependence and cooperation of the
5
6 terms in the distinct inverse-scattering subseries for free-surface multiple and internal
7
8 multiple removal: SEG Technical Program Expanded Abstract, pages 4561–4565.
9
10
11 Maston, K., Corrigan, D., Weglein, A., Yong, C. Y., and Carvalho, P., 1999, Inverse scatter-
12
13 ing internal multiple attenuation: Results from complex synthetic and field data examples:
14
15 SEG Expanded Abstract.
16
17
18
19 Matson, K. H., 1997, An inverse-scattering series method for attenuating elastic multiples
20
21 from multicomponent land and ocean bottom seismic data: Ph.D. thesis, University of
22
23 British Columbia.
24
25
26
27 Mayhan, J., and Weglein, A., 2013, First application of green's theorem-derived source
28
29 and receiver deghosting on deep-water gulf of mexico synthetic (seam) and field data:
30
31 Geophysics, **78**, no. 2, WA77–WA89.
32
33
34
35 Mayhan, J. D., 2013, Wave-theoretic preprocessing to allow the inverse scattering series
36
37 methods for multiple removal and depth imaging to realize their potential and impact:
38
39 Methods, examples, and added value: Ph.D. thesis, University of Houston.
40
41
42
43
44 Moses, H., 1956, Calculation of scattering potential from reflection coefficients: Phys. Rev.,
45
46 **102**, no. 2, 559–567.
47
48
49
50 Osen, A., Secrest, B. G., Amundsen, L., and Reitan, A., 1998, Wavelet estimation from
51
52 marine pressure measurements: Geophysics, **63**, 21082119.
53
54
55
56 Prosser, R. T., 1969, Formal solutions of inverse scattering problems: Journal of Mathe-
57
58 matical Physics, **10**, no. 10, 1819–1822.
59
60

- 1
2
3
4 Razavy, M., 1975, Determination of the wave velocity in an inhomogeneous medium from
5
6 reflection data: *J. Acoust. Soc. Am.*, **58**, 956–963.
7
8
9 Shen, Y., 2017, Wave-theory-based seismic data preprocessing: An extension of the current
10
11 deghosting method to allow for a variable measurement surface topography and its impact
12
13 on the inverse scattering series multiple removal: Ph.D. thesis, University of Houston.
14
15
16 Stolt, R. H., and Jacobs, B., 1980, Inversion of seismic data in a laterally heterogeneous
17
18 medium: *Stanford Exploration Project*, **24**.
19
20
21 Stolt, R. H., and Weglein, A. B., 1985, Migration and inversion of seismic data: *Geophysics*,
22
23 **50**, no. 12, 2458–2472.
24
25
26
27 Tan, T. H., 1999, Wavelet spectrum estimation: *Geophysics*, **64**, 18361846.
28
29
30 Taylor, J. R., 1972, *Scattering theory: the quantum theory of nonrelativistic collisions*:
31
32 John Wiley & Sons, Inc.
33
34
35 Verschuur, D. J., Berkhout, A. J., and Wapenaar, C. P. A., 1992, Adaptive surface-related
36
37 multiple elimination: *Geophysics*, **57**, 1166–1177.
38
39
40
41 Verschuur, D. J., 1991, *Surface-related multiple elimination, an inversion approach*: Ph.D.
42
43 thesis, Delft University of Technology.
44
45
46 Weglein, A., and Dragoset, W., 2005, *Multiple attenuation.*: *Geophysics reprint series Soc.*
47
48 *Expl. Geophys.*
49
50
51 Weglein, A. B., and Secret, B. G., July 1990, Wavelet estimation for a multidimensional
52
53 acoustic earth model: *Geophysics*, **55**, no. 7, 902–913.
54
55
56
57
58
59
60

1
2
3
4 Weglein, A. B., Boyce, W. E., and Anderson, J. E., 1981, Obtaining three-dimensional ve-
5
6 locity information directly from reflection seismic data: An inverse scattering formalism:
7
8 Geophysics, **46**, no. 8, 1116–1120.
9

10
11 Weglein, A. B., Gasparotto, F. A., Carvalho, P. M., and Stolt, R. H., November-December
12
13 1997, An inverse-scattering series method for attenuating multiples in seismic reflection
14
15 data: Geophysics, **62**, no. 6, 1975–1989.
16
17

18
19 Weglein, A. B., Matson, K. H., and Berkhout, A. J., 2000, Wave theoretic approaches
20
21 to multiple attenuation: Concepts, status, open issues, and plans: Part ii: Offshore
22
23 Technology Conference.
24
25

26
27 Weglein, A. B., Shaw, S. A., Matson, K. H., Sheiman, J. L., Stolt, R. H., Tan, T. H., Osen,
28
29 A., Correa, G. P., Innanen, K. A., Guo, Z., , and Zhang, J., 2002a, New approaches
30
31 to deghosting towedstreamer and oceanbottom pressure measurements: SEG Expanded
32
33 Abstracts, pages 2114–2117.
34
35

36
37 ——— 2002b, New approaches to deghosting towed-streamer and ocean-bottem pressure
38
39 measurements: 72nd Annual International Meeting, SEG, Expanded Abstracts, pages
40
41 1016–1019.
42
43

44
45 Weglein, A. B., Araujo, F. V., Carvalho, P. M., Stolt, R. H., Matson, K. H., Coates, R. T.,
46
47 Corrigan, D., Foster, D. J., Shaw, S. A., and Zhang, H., 2003, Inverse scattering series
48
49 and seismic exploration: Inverse Problems, **19**, no. 6, R27–R83.
50

51
52 Weglein, A., 2012, Short note: an alternative subtraction criteria (to energy minimization)
53
54 for free-surface multiple removal: Mission-Oriented Seismic Research Program (M-OSRP)
55
56 Annual Report.
57
58
59
60

- 1
2
3
4 Weglein, A. B., 2016, Multiple:signal or noise?: Geophysics, **81**, no. 4, v283–v302.
5
6
7 Weglein, A. B., 2017, A direct inverse method for subsurface properties: The conceptual
8
9 and practical benefit and added value in comparison with all current indirect methods,
10
11 for example, amplitude-variation-with-offset and full-waveform inversion: Interpretation,
12
13 **5**, no. 3, SL89–SL107.
14
15
16
17 Weglein, A., 2018, A new and comprehensive perspective on the role of primaries and mul-
18
19 tiple in seismic data processing structure determination and amplitude analysis: Journal
20
21 of Seismic Exploration, page Submitted.
22
23
24 Wu, J., and Weglein, A., 2014, Elastic green’s theorem preprocessing for on-shore internal
25
26 multiple attenuation: Theory and initial synthetic data tests: SEG Technical Program
27
28 Expanded Abstract, pages 4299–4304.
29
30
31
32 Wu, J., and Weglein, A., 2015, Preprocessing in displacement space for on-shore seismic
33
34 processing: removing ground roll and ghosts without damaging the reflection data: SEG
35
36 Technical Program Expanded Abstract, pages 4626–4630.
37
38
39 Wu, J., and Weglein, A., 2016a, Green’s theorem-based onshore preprocessing: A reduced
40
41 data requirement assuming a vacuum/earth model for the air/earth interface and the
42
43 evaluation of the usefulness of that assumption: SEG Technical Program Expanded Ab-
44
45 stract, pages 4685–4689.
46
47
48
49 ——— 2016b, Predicting deghosted reflection data for both pressure and multicomponent
50
51 displacements at the ocean bottom: SEG Technical Program Expanded Abstract, pages
52
53 4751–4755.
54
55
56
57 Wu, J., and Weglein, A., 2017, A new method for deghosting data collected on a depth-
58
59
60

1
2
3
4 variable acquisition surface by combining green's theorem wave separation followed by
5
6 a stolt extended claerbout iii wave prediction for one-way propagating waves.: SEG
7
8 Expanded Abstracts, pages 4859–4864.
9

10
11 Zhang, H., and Shaw, S., 2010, 1-D analytical analysis of higher order internal multiples
12
13 predicted via the inverse scattering series based algorithm: SEG Technical Program Ex-
14
15 panded Abstracts, **29**, 3493–3498.
16
17

18
19 Zhang, J., 2007, Wave theory based data preparation for inverse scattering multiple removal,
20
21 depth imaging and parameter estimation: Analysis and numerical tests of green's theorem
22
23 deghosting theory: Ph.D. thesis, University of Houston.
24
25

26
27 Zhang, Z., 2017, Impact of the topography of the acquisition surface on preprocessing
28
29 and subsequent free surface multiple elimination and depth migration: Examining the
30
31 issue and providing a preprocessing response that accommodates a variable topography
32
33 - thereby allowing subsequent multiple removal and imaging methods to deliver their
34
35 promise and potential: Ph.D. thesis, University of Houston.
36
37
38
39
40
41
42
43
44
45
46
47
48
49
50
51
52
53
54
55
56
57
58
59
60

LIST OF FIGURES

1
2
3
4
5
6
7
8
9
10
11
12
13
14
15
16
17
18
19
20
21
22
23
24
25
26
27
28
29
30
31
32
33
34
35
36
37
38
39
40
41
42
43
44
45
46
47
48
49
50
51
52
53
54
55
56
57
58
59
60

1 Illustration of different seismic events in marine environment. Yellow solid line: reference waves; Green and light blue dashed: source ghost and receiver ghost, respectively; Dark blue dashed line: free surface multiple; Orange dashed line: internal multiple; solid black line: primary.

2 ISS free-surface multiple prediction algorithm and SRME free-surface multiple prediction algorithm

3 Three sets of comparisons between the ISS free-surface multiple prediction and SRME free-surface multiple prediction

4 A 1D subsurface model with a horizontal reflector and a free-surface.

5 Input data for the ISS free-surface multiple prediction. Notice that, only primaries and free-surface multiples are generated for ISS FSME input.

6 Input data for the SRME free-surface multiple prediction. Notice that, primaries and free-surface multiples and their source ghosts are generated for SRME input

7 ISS free-surface multiple prediction (D'_2 in equation 1) with the input in figure 5.

8 SRME free-surface multiple prediction (equation 3) with the input in figure 6.

9 A trace comparison at 500m offset between the input of the ISS FSME and its prediction. The red and blue line represent input data to the ISS FSME and its prediction, respectively. We can see the ISS free-surface multiple prediction agrees with the actual free-surface multiple very well. Notice that, the predicted free-surface multiple has opposite sign compared with the actual free-surface multiple, we first flip the polarity of the prediction, then compare it with the actual data for easy comparison.

10 A trace comparison at 500m offset between the input of the SRME and its prediction. The red and blue represent the input data to the SRME and its prediction for

1
2
3
4 free-surface multiples, respectively. We can see from this trace comparison, the SRME pro-
5
6
7 vides an approximate free-surface multiple prediction.

8
9 11 A 1D subsurface model with two primary events and one free-surface multiple
10
11 event.

12
13 12 Input data generated based on the model shown in figure 11.

14
15 13 Prediction of free-surface multiple by the ISS FSME (D'_2 in equation 1) using the
16
17 input data shown in figure 12.

18
19
20 14 Prediction of free-surface multiple by the SRME using the input data shown in
21
22 figure 12.

23
24 15 Free-surface multiple removal result after directly subtracting the ISS prediction
25
26 result (figure 13) from the data (figure 12).

27
28
29 16 Free-surface multiple removal result by combing the SRME prediction (figure 14)
30
31 and adaptive subtraction.

32
33 17 Actual primaries in the data shown in figure 12.

34
35 18 Trace comparison at Offset 100m. Red, blue and green line represent actual data,
36
37 ISS free-surface multiple prediction and SRME prediction, respectively.

38
39
40 19 Trace comparison at Offset 500m. Red, blue and green line represent actual data,
41
42 ISS free-surface multiple prediction and SRME prediction, respectively.

43
44 20 Trace comparison at Offset 750m. Red, blue and green line represent actual data,
45
46 ISS free-surface multiple prediction and SRME prediction, respectively.

47
48
49 21 Trace comparison at Offset 1000m. Red, blue and green line represent actual data,
50
51 ISS free-surface multiple prediction and SRME prediction, respectively.

52
53
54 22 Trace comparison at Offset 1250m. Red, blue and green line represent actual data,
55
56 ISS free-surface multiple prediction and SRME prediction, respectively.

1
2
3
4 23 Trace comparison at Offset 750m. Red, blue and green represent the actual pri-
5
6
7 mary, result after ISS FSME and result after the SRME + adaptive, respectively.

8
9 24 Input data with random noise added on the analytic data.

10
11 25 Prediction of free-surface multiple by the ISS FSME (D'_2 in equation 1) using the
12
13 input data shown in figure 24.

14
15 26 Prediction of free-surface multiple by the SRME using the input data shown in
16
17 figure 24.

18
19
20 27 Free-surface multiple removal result after directly subtracting the ISS prediction
21
22 result (figure 25) from the data (figure 24).

23
24 28 Free-surface multiple removal result by combing the SRME prediction (figure 26)
25
26 and adaptive subtraction.

27
28
29 29 Actual primaries in the data shown in figure 24.

30
31 30 Trace comparison at Offset 100m. Red, blue and green line represent actual data,
32
33 ISS free-surface multiple prediction and SRME prediction, respectively.

34
35
36 31 Trace comparison at Offset 500m. Red, blue and green line represent actual data,
37
38 ISS free-surface multiple prediction and SRME prediction, respectively.

39
40 32 Trace comparison at Offset 750m. Red, blue and green line represent actual data,
41
42 ISS free-surface multiple prediction and SRME prediction, respectively.

43
44 33 Trace comparison at Offset 1000m. Red, blue and green line represent actual data,
45
46 ISS free-surface multiple prediction and SRME prediction, respectively.

47
48
49 34 Trace comparison at Offset 1250m. Red, blue and green line represent actual data,
50
51 ISS free-surface multiple prediction and SRME prediction, respectively.

52
53
54 35 Trace comparison at Offset 750m. Red, blue and green represent the actual pri-
55
56 mary, result after ISS FSME and result after the SRME + adaptive, respectively.

- 1
2
3
4 36 Input data generated from an absorptive medium.
5
6 37 Prediction of free-surface multiple by the ISS FSME (D_2' in equation 1) using the
7
8 input data generated by an absorptive medium shown in figure 36.
9
10 38 Prediction of free-surface multiple by the SRME using the input data generated
11
12 by an absorptive medium shown in figure 36.
13
14 39 Free-surface multiple removal result after directly subtracting the ISS prediction
15
16 result (figure 37) from the data (figure 36).
17
18 40 Free-surface multiple removal result by combing the SRME prediction (figure 38)
19
20 and adaptive subtraction.
21
22 41 Actual primaries in the input data shown in figure 36.
23
24 42 Trace comparison at Offset 100m. Red, blue and green line represent actual data,
25
26 ISS free-surface multiple prediction and SRME prediction, respectively.
27
28 43 Trace comparison at Offset 500m. Red, blue and green line represent actual data,
29
30 ISS free-surface multiple prediction and SRME prediction, respectively.
31
32 44 Trace comparison at Offset 750m. Red, blue and green line represent actual data,
33
34 ISS free-surface multiple prediction and SRME prediction, respectively.
35
36 45 Trace comparison at Offset 1000m. Red, blue and green line represent actual data,
37
38 ISS free-surface multiple prediction and SRME prediction, respectively.
39
40 46 Trace comparison at Offset 1250m. Red, blue and green line represent actual data,
41
42 ISS free-surface multiple prediction and SRME prediction, respectively.
43
44 47 Trace comparison at Offset 750m. Red, blue and green represent the actual pri-
45
46 mary, result after ISS FSME and result after the SRME + adaptive, respectively.
47
48
49
50
51
52
53 A-1 Green's function G_0^{fs} , travels up from the source to the free-surface and then down
54
55 to the receiver.
56
57
58
59
60

1
2
3
4 A-2 Model used to generated data in Zhang (2007) to test the ISS FSME.
5

6 A-3 A trace comparison between the input data D'_1 (solid line) to the ISS FSME and
7
8 output data $D'_1 + D'_2$ after the ISS FSME. When D'_2 is added to D'_1 , two things happen,
9
10 the first-order free-surface multiple is eliminated, all higher-order free-surface multiples are
11
12 altered, and prepared for their removal by D'_3, D'_4 , etc.
13
14

15 B-1 (a) Monopole source and its 2D Green's function in k_x, ω domain. (b) Dipole
16
17 source and its 2D Green's function. (c) Monopole source & its source ghosts and their 2D
18
19 Green's functions. Free-surface is at depth $z = 0$. $q = \sqrt{\frac{\omega^2}{c_0^2} - k_x^2}$, where ω, k_x and c_0 are
20
21 the temporal frequency, horizontal wavenumber, and medium velocity.
22
23
24
25
26
27
28
29
30
31
32
33
34
35
36
37
38
39
40
41
42
43
44
45
46
47
48
49
50
51
52
53
54
55
56
57
58
59
60

1
2
3
4
5
6
7
8
9
10
11
12
13
14
15
16
17
18
19
20
21
22
23
24
25
26
27
28
29
30
31
32
33
34
35
36
37
38
39
40
41
42
43
44
45
46
47
48
49
50
51
52
53
54
55
56
57
58
59
60

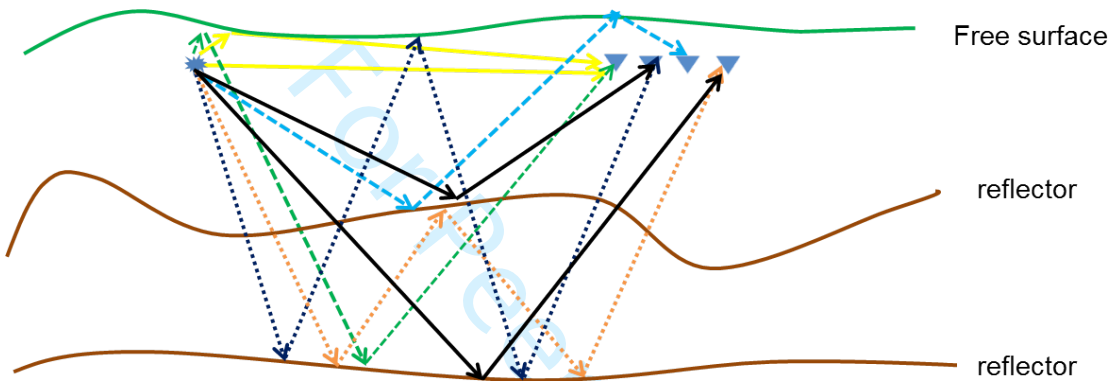


Figure 1: Illustration of different seismic events in marine environment. Yellow solid line: reference waves; Green and light blue dashed: source ghost and receiver ghost, respectively; Dark blue dashed line: free surface multiple; Orange dashed line: internal multiple; solid black line: primary.

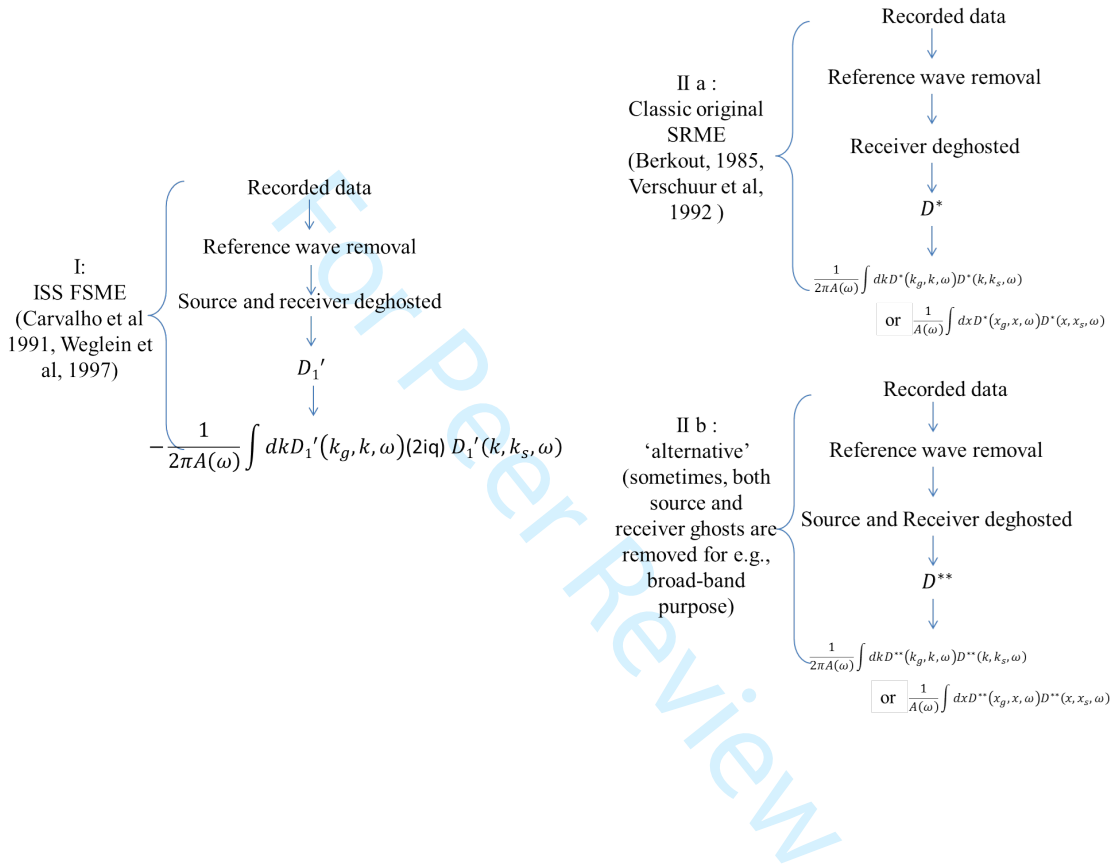


Figure 2: ISS free-surface multiple prediction algorithm and SRME free-surface multiple prediction algorithm

Examples

- 1st set of comparisons:
 - I and II a (without noise, without absorptive, isolated free-surface multiple and primary)
- 2nd set of comparisons:
 - I and II b (without noise, without absorptive, interfering free-surface multiple and primary)
 - I and II b (with noise, without absorptive, interfering free-surface multiple and primary)
- 3rd set of comparisons:
 - I and II b (without noise, with absorptive, interfering free-surface multiple and primary)

Figure 3: Three sets of comparisons between the ISS free-surface multiple prediction and SRME free-surface multiple prediction

–

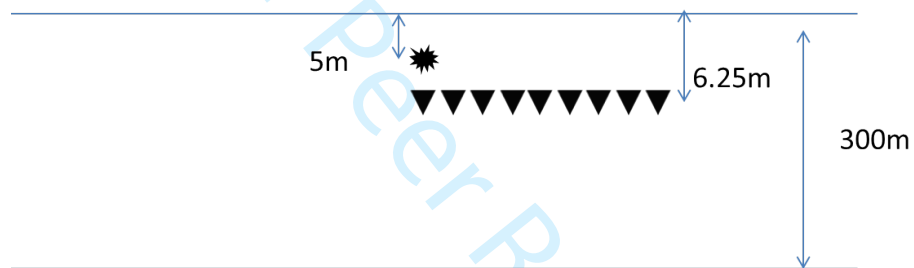


Figure 4: A 1D subsurface model with a horizontal reflector and a free-surface. –

1
2
3
4
5
6
7
8
9
10
11
12
13
14
15
16
17
18
19
20
21
22
23
24
25
26
27
28
29
30
31
32
33
34
35
36
37
38
39
40
41
42
43
44
45
46
47
48
49
50
51
52
53
54
55
56
57
58
59
60

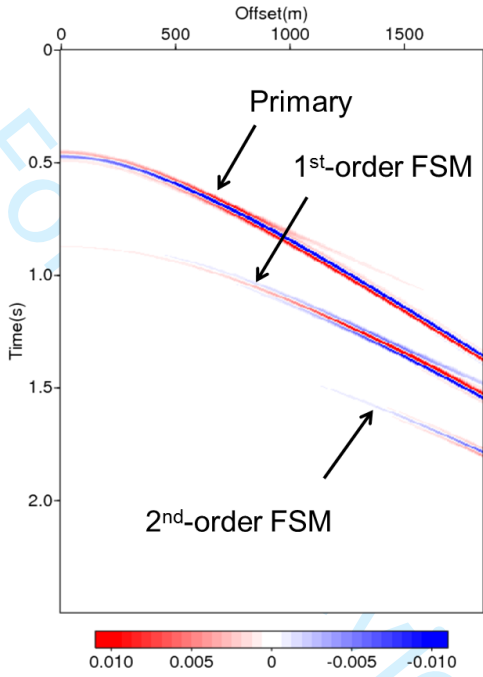


Figure 5: Input data for the ISS free-surface multiple prediction. Notice that, only primaries and free-surface multiples are generated for ISS FSME input.

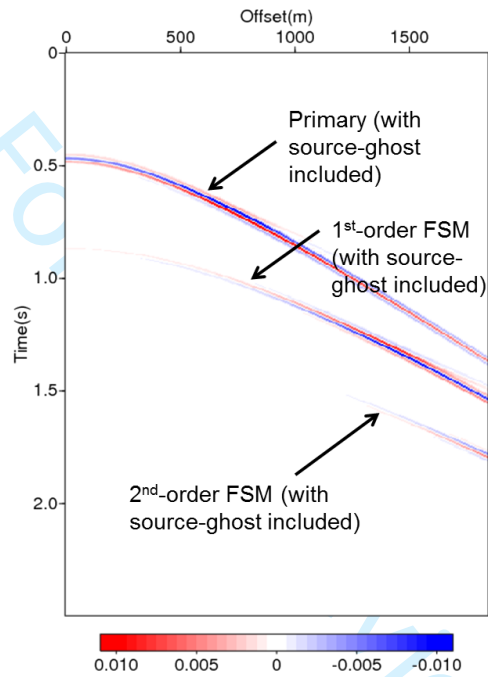


Figure 6: Input data for the SRME free-surface multiple prediction. Notice that, primaries and free-surface multiples and their source ghosts are generated for SRME input

1
2
3
4
5
6
7
8
9
10
11
12
13
14
15
16
17
18
19
20
21
22
23
24
25
26
27
28
29
30
31
32
33
34
35
36
37
38
39
40
41
42
43
44
45
46
47
48
49
50
51
52
53
54
55
56
57
58
59
60

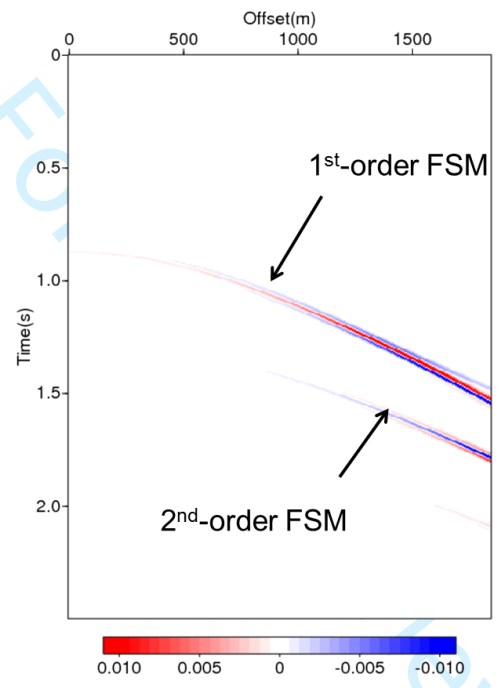


Figure 7: ISS free-surface multiple prediction (D'_2 in equation 1) with the input in figure 5.

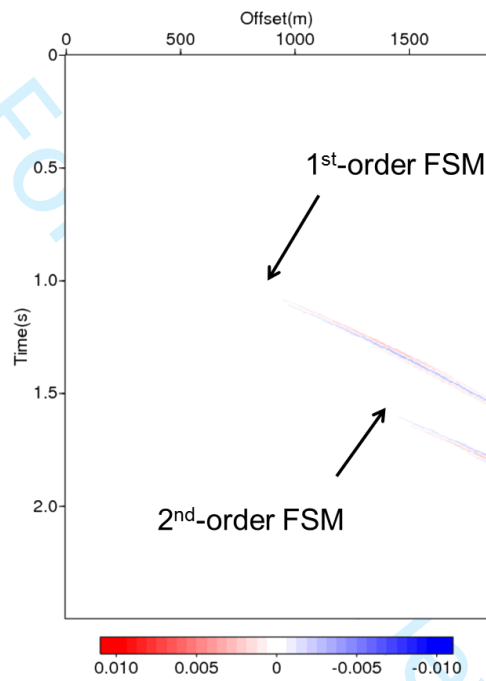


Figure 8: SRME free-surface multiple prediction (equation 3) with the input in figure 6.

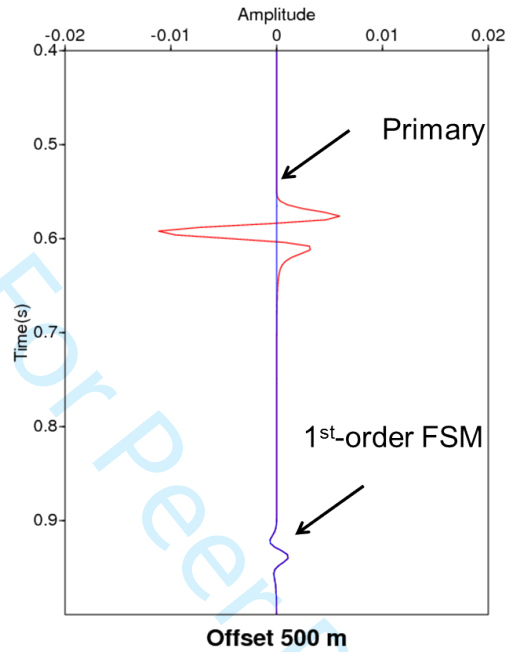


Figure 9: A trace comparison at 500m offset between the input of the ISS FSME and its prediction. The red and blue line represent input data to the ISS FSME and its prediction, respectively. We can see the ISS free-surface multiple prediction agrees with the actual free-surface multiple very well. Notice that, the predicted free-surface multiple has opposite sign compared with the actual free-surface multiple, we first flip the polarity of the prediction, then compare it with the actual data for easy comparison.

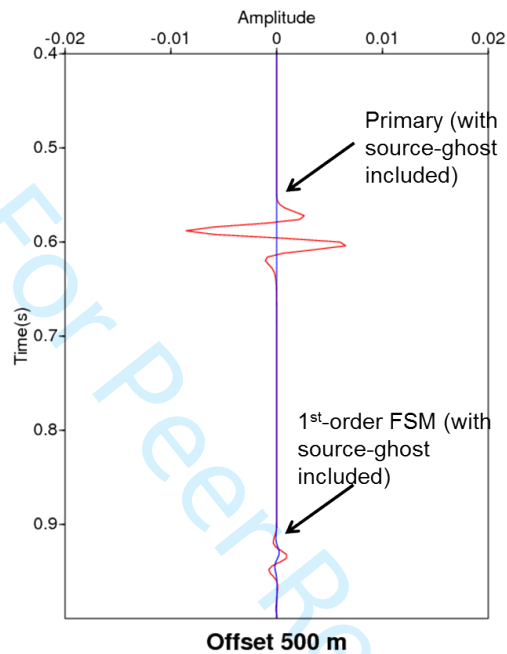


Figure 10: A trace comparison at 500m offset between the input of the SRME and its prediction. The red and blue represent the input data to the SRME and its prediction for free-surface multiples, respectively. We can see from this trace comparison, the SRME provides an approximate free-surface multiple prediction.

—

1
2
3
4
5
6
7
8
9
10
11
12
13
14
15
16
17
18
19
20
21
22
23
24
25
26
27
28
29
30
31
32
33
34
35
36
37
38
39
40
41
42
43
44
45
46
47
48
49
50
51
52
53
54
55
56
57
58
59
60

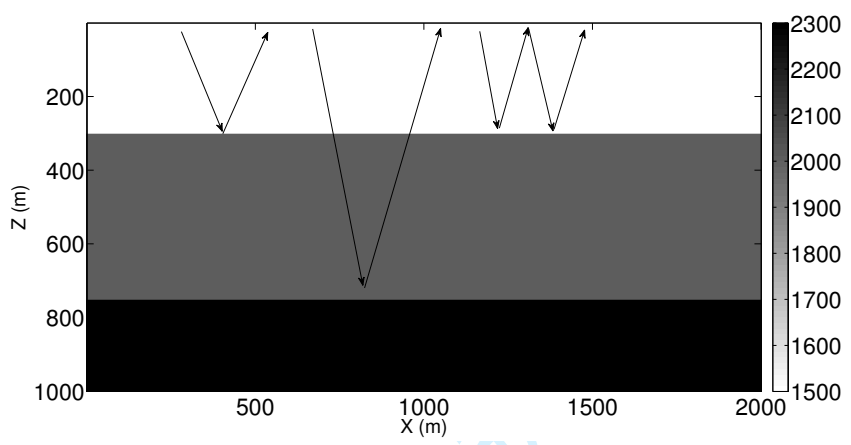


Figure 11: A 1D subsurface model with two primary events and one free-surface multiple event.

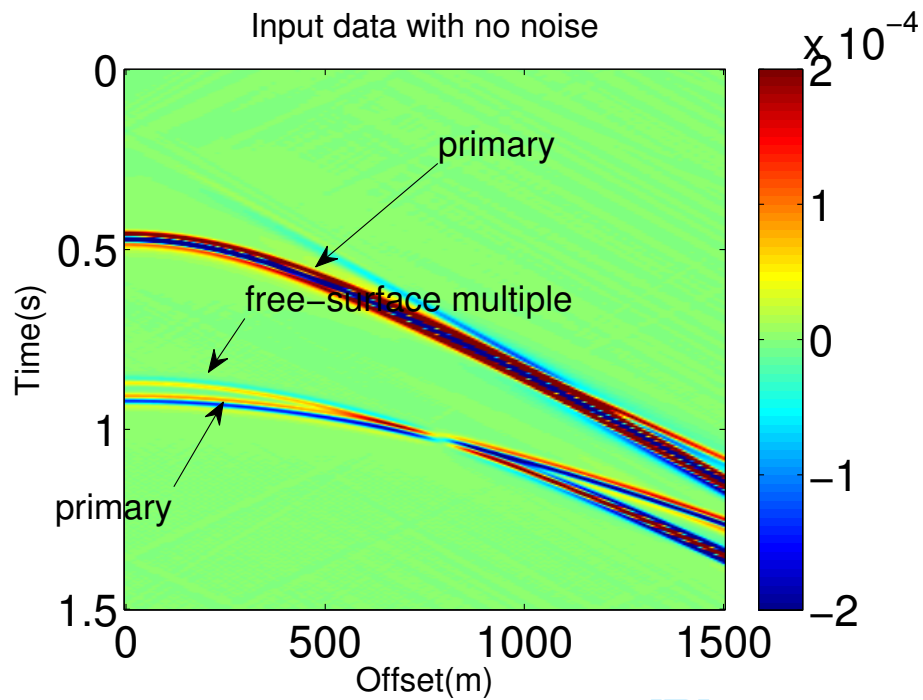


Figure 12: Input data generated based on the model shown in figure 11. -

1
2
3
4
5
6
7
8
9
10
11
12
13
14
15
16
17
18
19
20
21
22
23
24
25
26
27
28
29
30
31
32
33
34
35
36
37
38
39
40
41
42
43
44
45
46
47
48
49
50
51
52
53
54
55
56
57
58
59
60

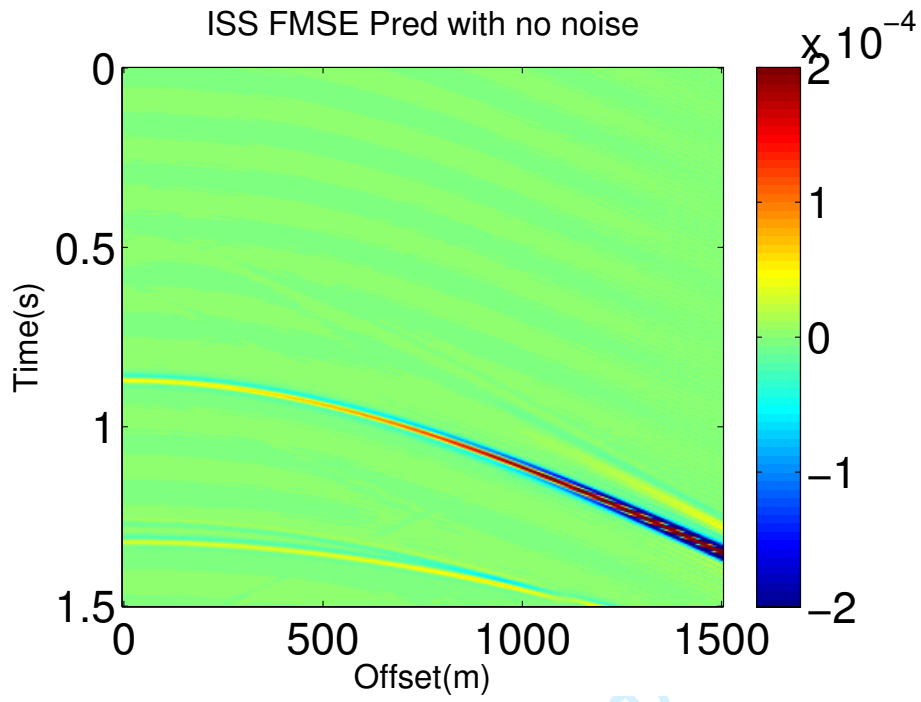
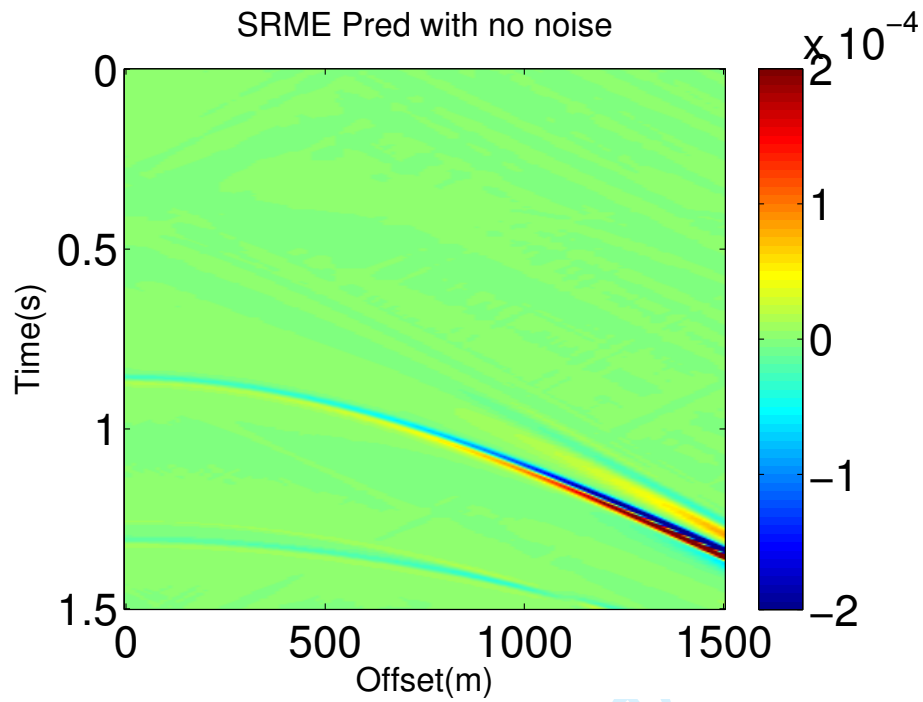


Figure 13: Prediction of free-surface multiple by the ISS FSME (D'_2 in equation 1) using the input data shown in figure 12.



42 Figure 14: Prediction of free-surface multiple by the SRME using the input data shown in
43 figure 12.
44
45

46 -

1
2
3
4
5
6
7
8
9
10
11
12
13
14
15
16
17
18
19
20
21
22
23
24
25
26
27
28
29
30
31
32
33
34
35
36
37
38
39
40
41
42
43
44
45
46
47
48
49
50
51
52
53
54
55
56
57
58
59
60

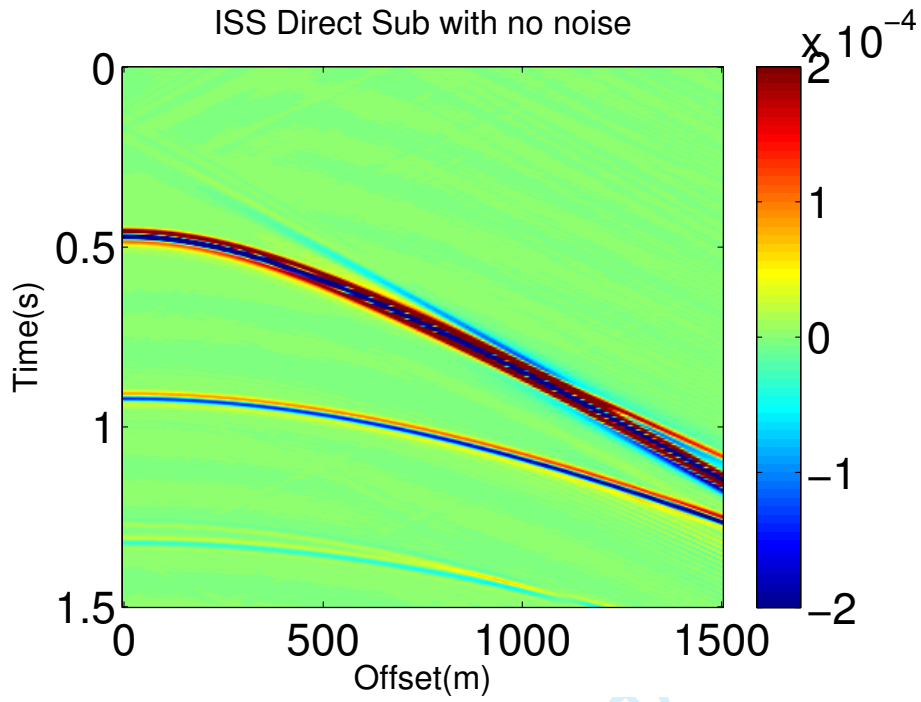
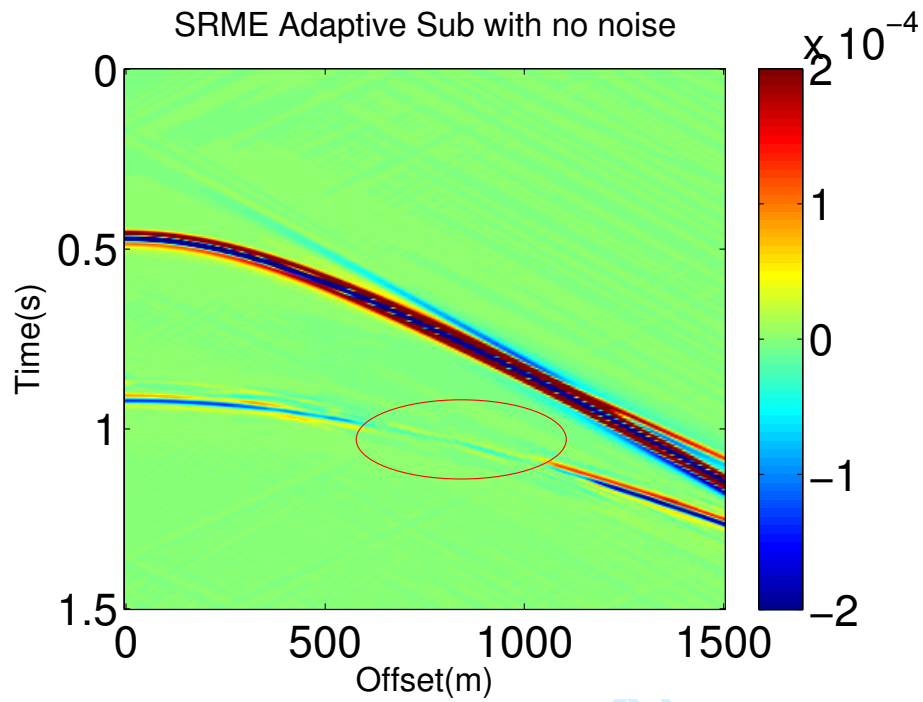


Figure 15: Free-surface multiple removal result after directly subtracting the ISS prediction result (figure 13) from the data (figure 12).



42 Figure 16: Free-surface multiple removal result by combing the SRME prediction (figure
43 14) and adaptive subtraction.
44
45

46 -

1
2
3
4
5
6
7
8
9
10
11
12
13
14
15
16
17
18
19
20
21
22
23
24
25
26
27
28
29
30
31
32
33
34
35
36
37
38
39
40
41
42
43
44
45
46
47
48
49
50
51
52
53
54
55
56
57
58
59
60

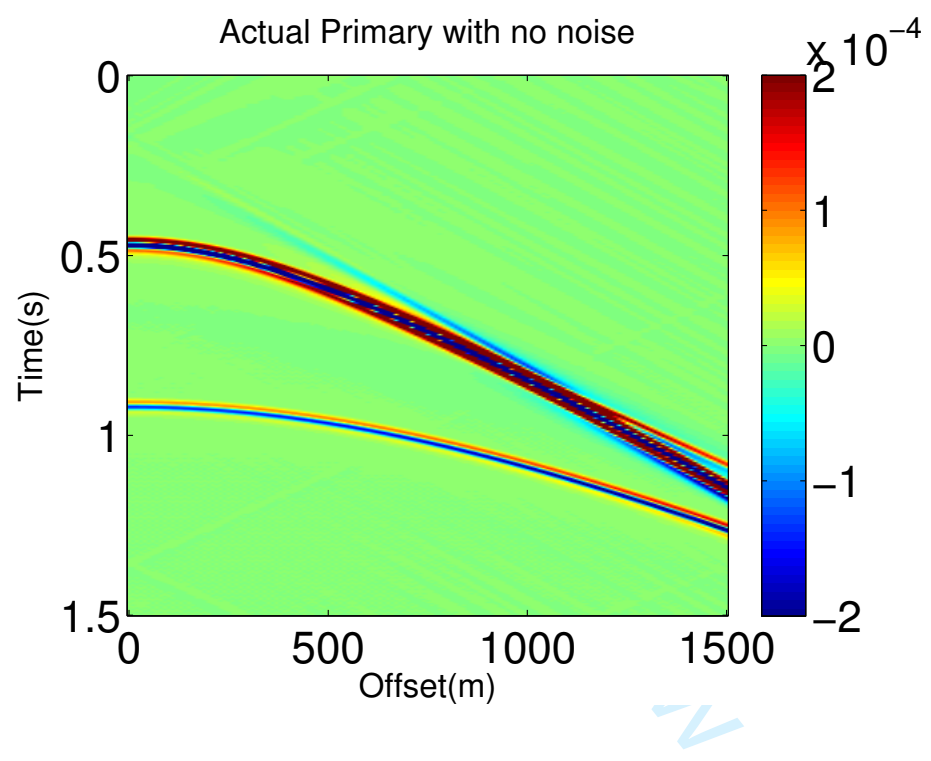
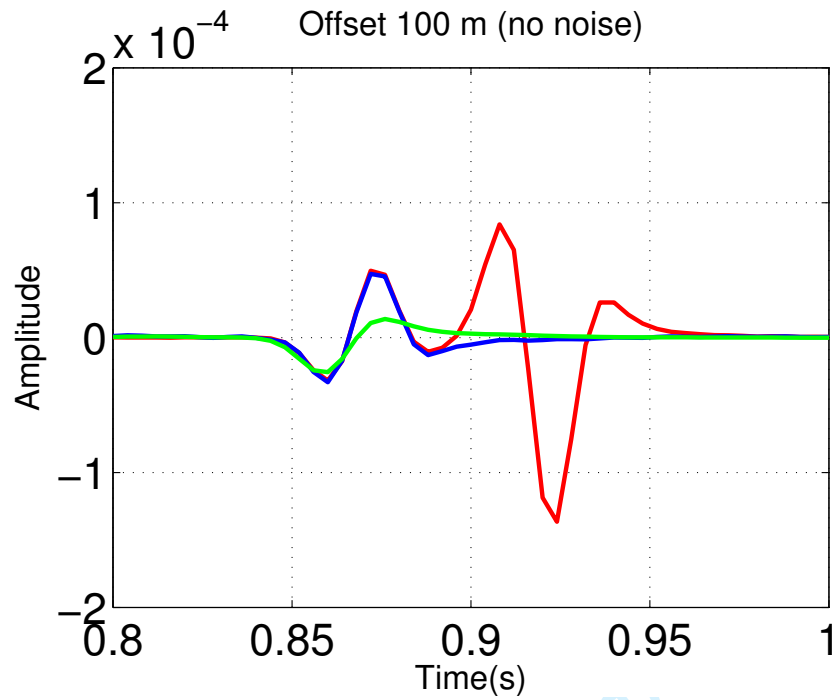


Figure 17: Actual primaries in the data shown in figure 12. –



42 Figure 18: Trace comparison at Offset 100m. Red, blue and green line represent actual
43 data, ISS free-surface multiple prediction and SRME prediction, respectively.
44
45

1
2
3
4
5
6
7
8
9
10
11
12
13
14
15
16
17
18
19
20
21
22
23
24
25
26
27
28
29
30
31
32
33
34
35
36
37
38
39
40
41
42
43
44
45
46
47
48
49
50
51
52
53
54
55
56
57
58
59
60

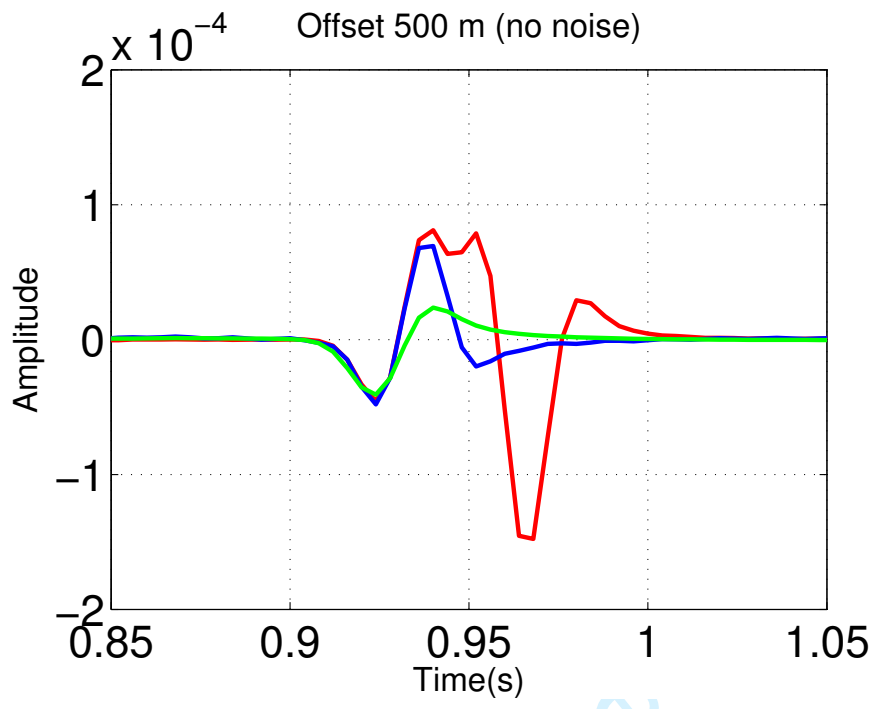


Figure 19: Trace comparison at Offset 500m. Red, blue and green line represent actual data, ISS free-surface multiple prediction and SRME prediction, respectively.

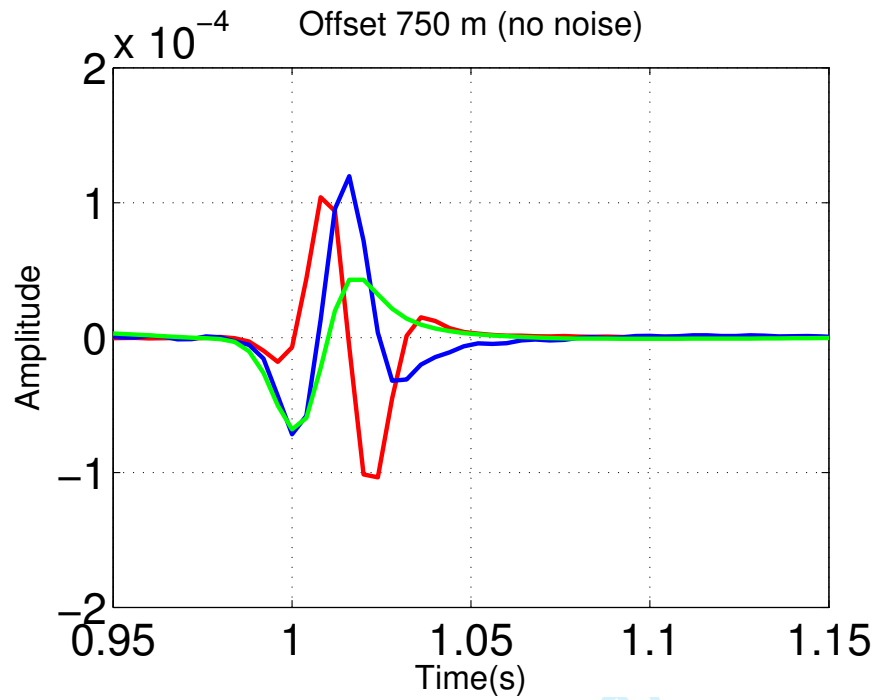


Figure 20: Trace comparison at Offset 750m. Red, blue and green line represent actual data, ISS free-surface multiple prediction and SRME prediction, respectively.

1
2
3
4
5
6
7
8
9
10
11
12
13
14
15
16
17
18
19
20
21
22
23
24
25
26
27
28
29
30
31
32
33
34
35
36
37
38
39
40
41
42
43
44
45
46
47
48
49
50
51
52
53
54
55
56
57
58
59
60

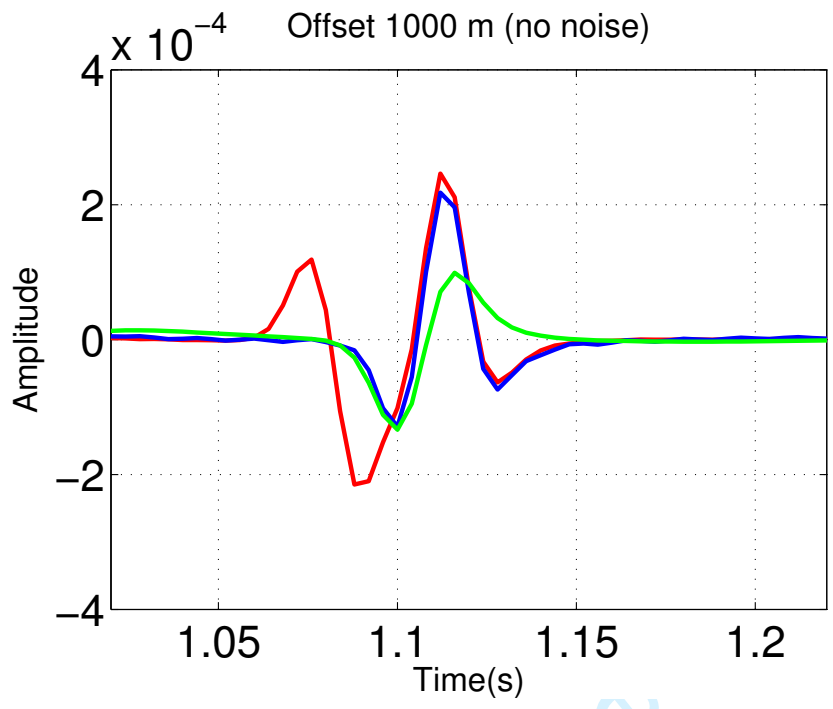
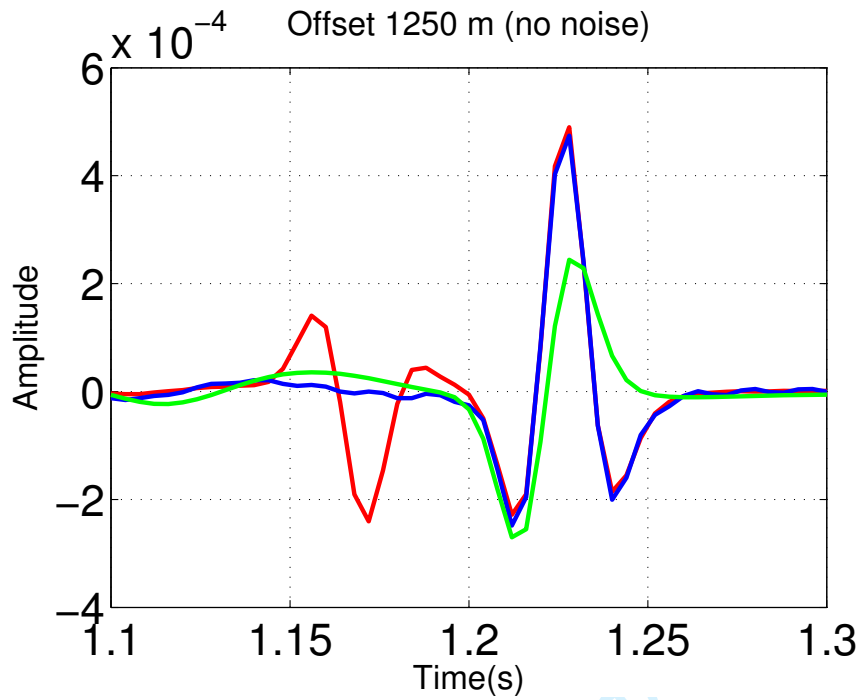


Figure 21: Trace comparison at Offset 1000m. Red, blue and green line represent actual data, ISS free-surface multiple prediction and SRME prediction, respectively.



42 Figure 22: Trace comparison at Offset 1250m. Red, blue and green line represent actual
43 data, ISS free-surface multiple prediction and SRME prediction, respectively.
44
45
46
47
48
49
50
51
52
53
54
55
56
57
58
59
60

1
2
3
4
5
6
7
8
9
10
11
12
13
14
15
16
17
18
19
20
21
22
23
24
25
26
27
28
29
30
31
32
33
34
35
36
37
38
39
40
41
42
43
44
45
46
47
48
49
50
51
52
53
54
55
56
57
58
59
60

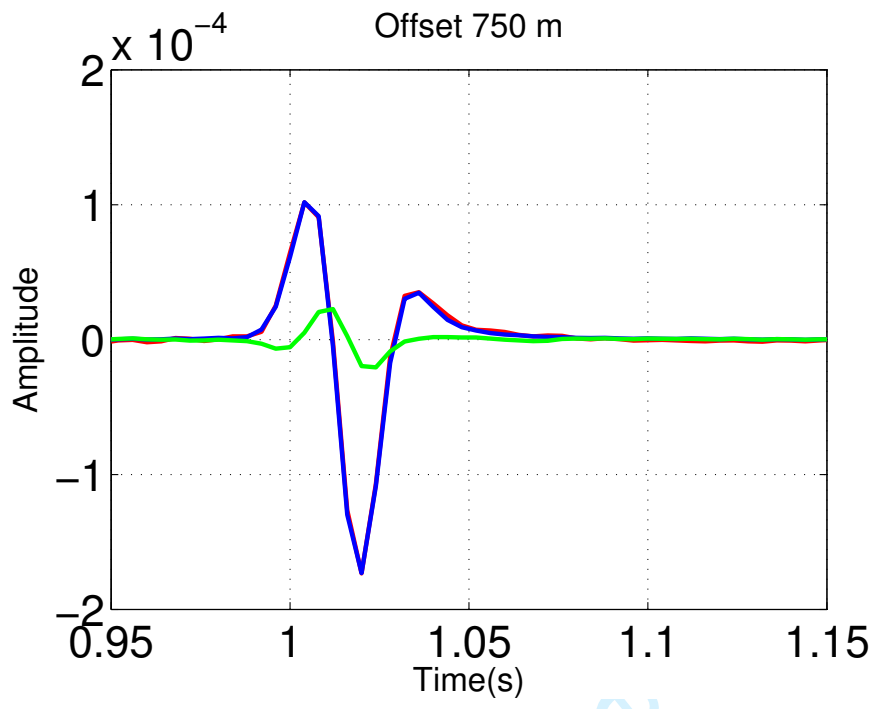


Figure 23: Trace comparison at Offset 750m. Red, blue and green represent the actual primary, result after ISS FSME and result after the SRME + adaptive, respectively.

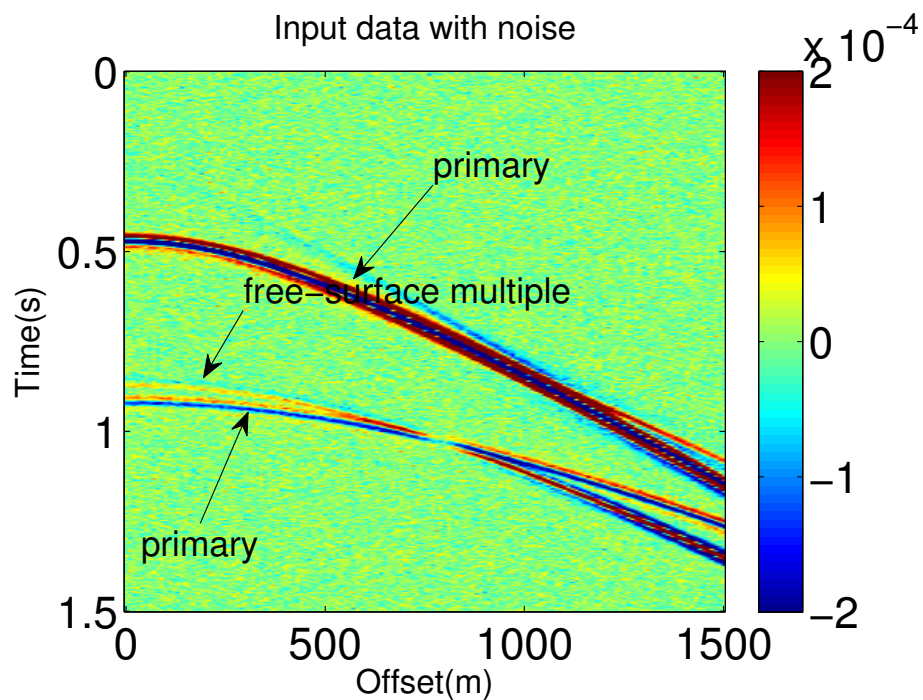


Figure 24: Input data with random noise added on the analytic data. –

1
2
3
4
5
6
7
8
9
10
11
12
13
14
15
16
17
18
19
20
21
22
23
24
25
26
27
28
29
30
31
32
33
34
35
36
37
38
39
40
41
42
43
44
45
46
47
48
49
50
51
52
53
54
55
56
57
58
59
60

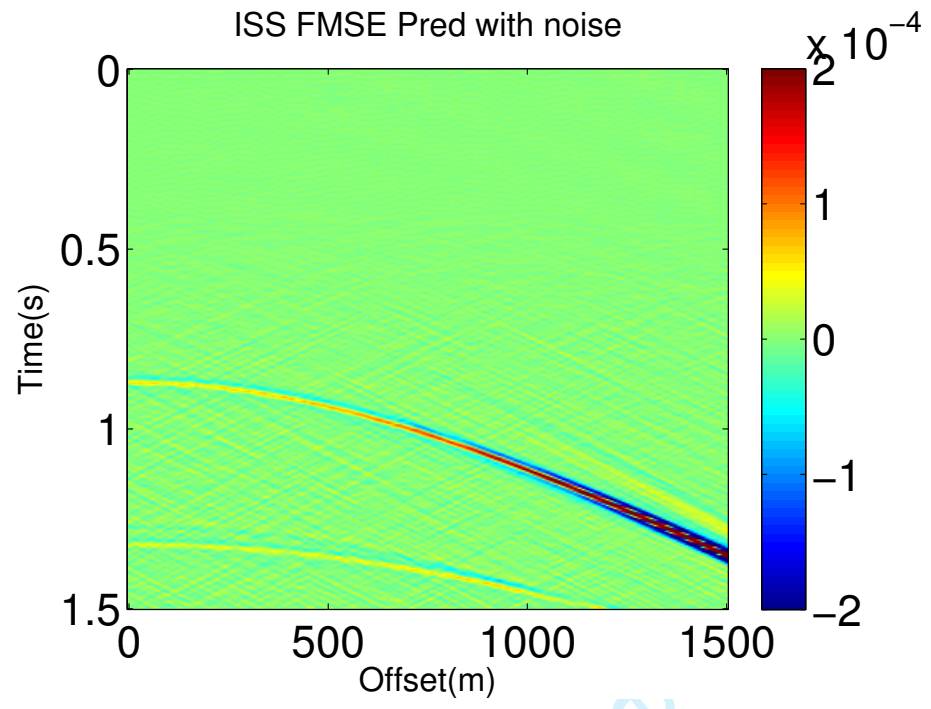
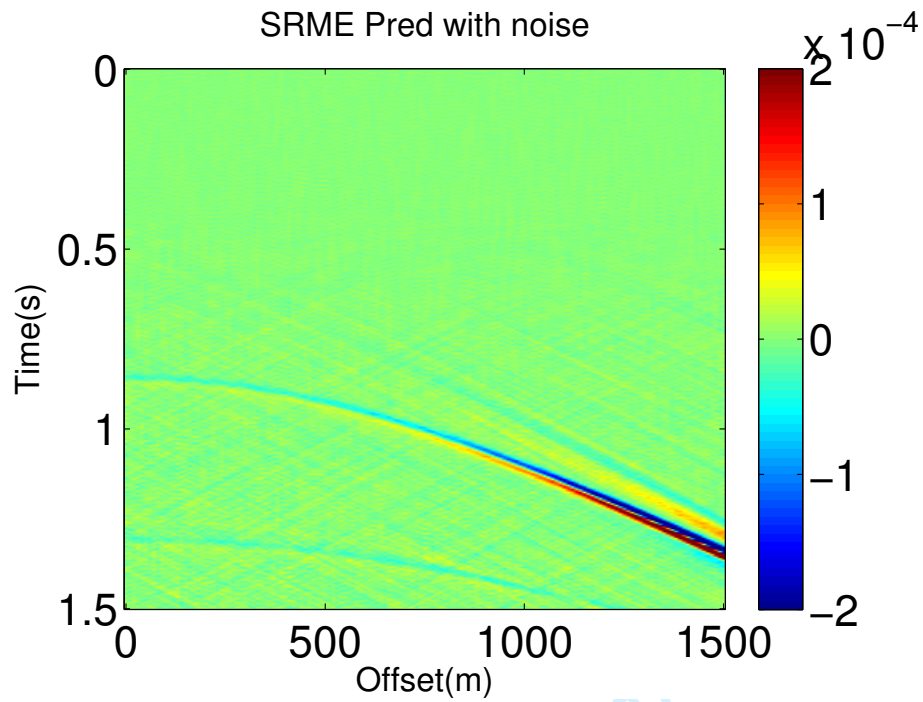


Figure 25: Prediction of free-surface multiple by the ISS FSME (D'_2 in equation 1) using the input data shown in figure 24.



42 Figure 26: Prediction of free-surface multiple by the SRME using the input data shown in
43 figure 24.
44
45

1
2
3
4
5
6
7
8
9
10
11
12
13
14
15
16
17
18
19
20
21
22
23
24
25
26
27
28
29
30
31
32
33
34
35
36
37
38
39
40
41
42
43
44
45
46
47
48
49
50
51
52
53
54
55
56
57
58
59
60

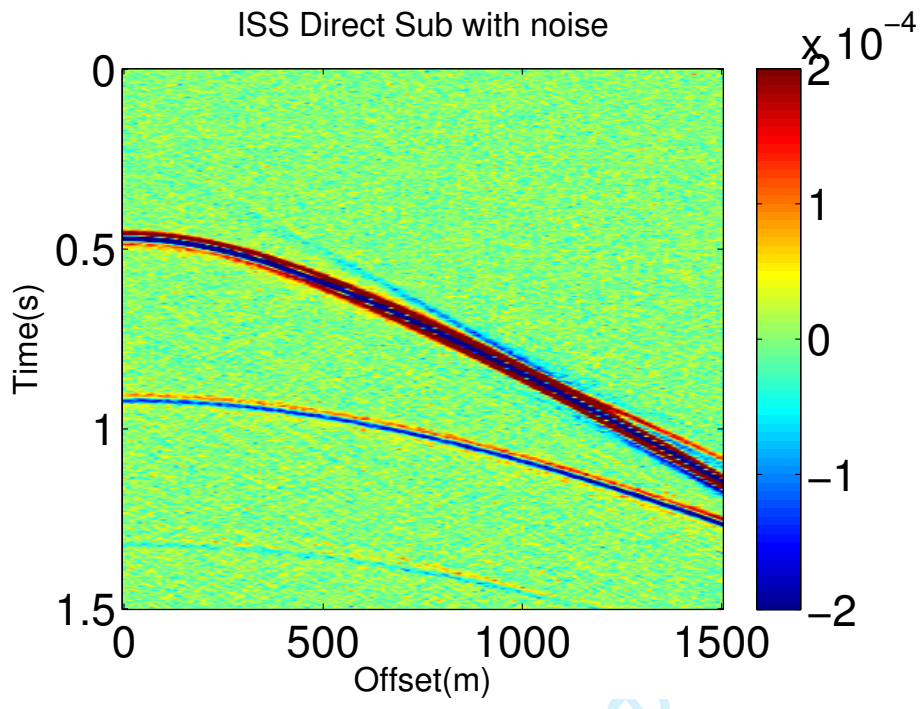
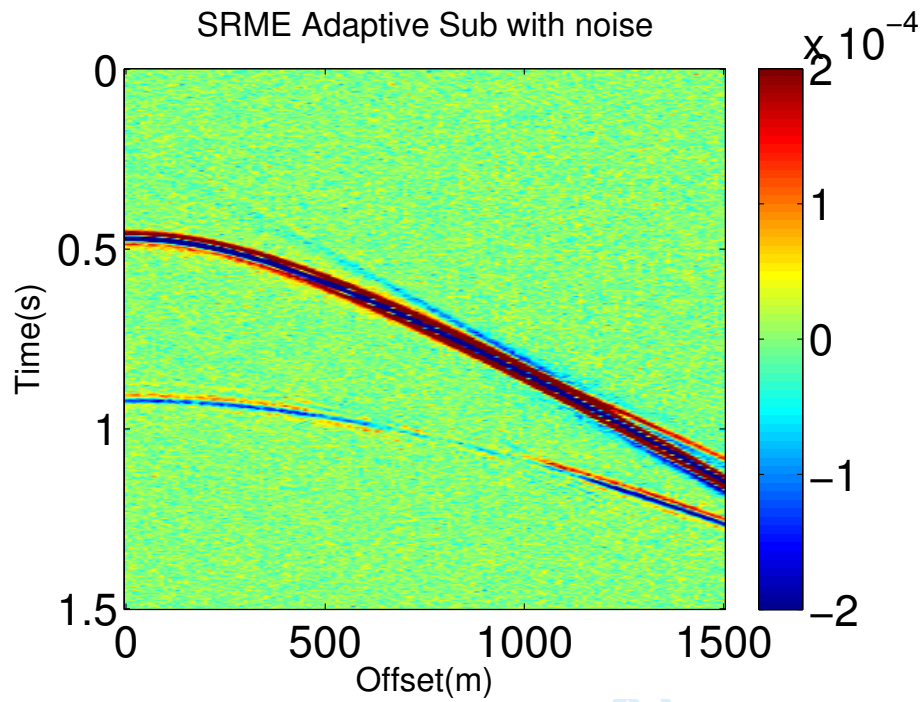


Figure 27: Free-surface multiple removal result after directly subtracting the ISS prediction result (figure 25) from the data (figure 24).



42 Figure 28: Free-surface multiple removal result by combing the SRME prediction (figure
43 26) and adaptive subtraction.
44
45

46 —

1
2
3
4
5
6
7
8
9
10
11
12
13
14
15
16
17
18
19
20
21
22
23
24
25
26
27
28
29
30
31
32
33
34
35
36
37
38
39
40
41
42
43
44
45
46
47
48
49
50
51
52
53
54
55
56
57
58
59
60

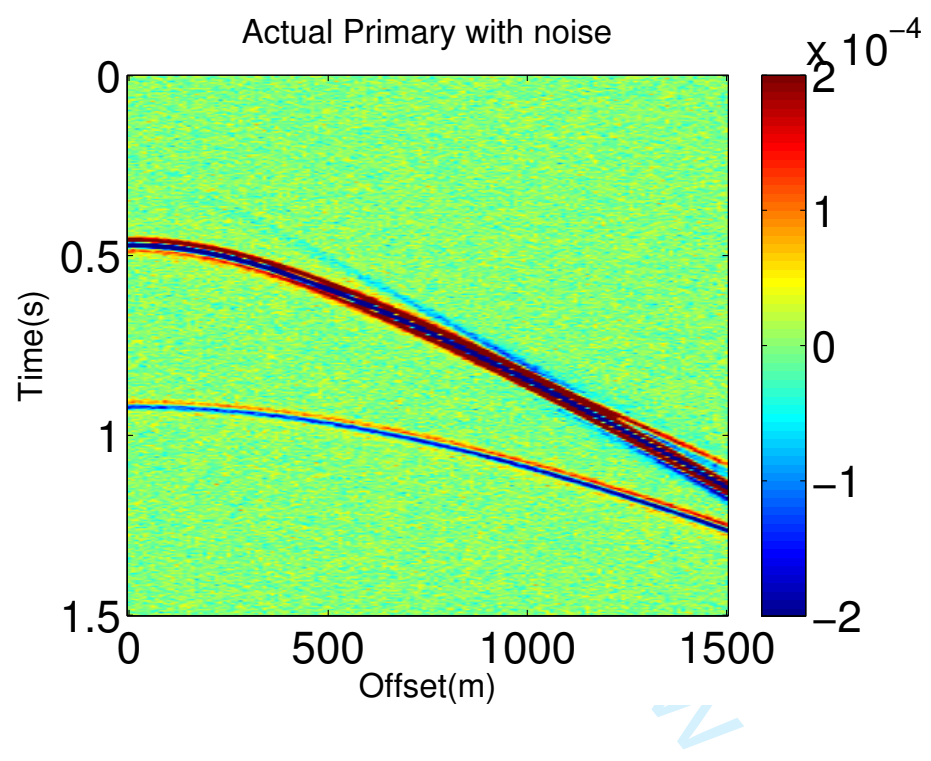
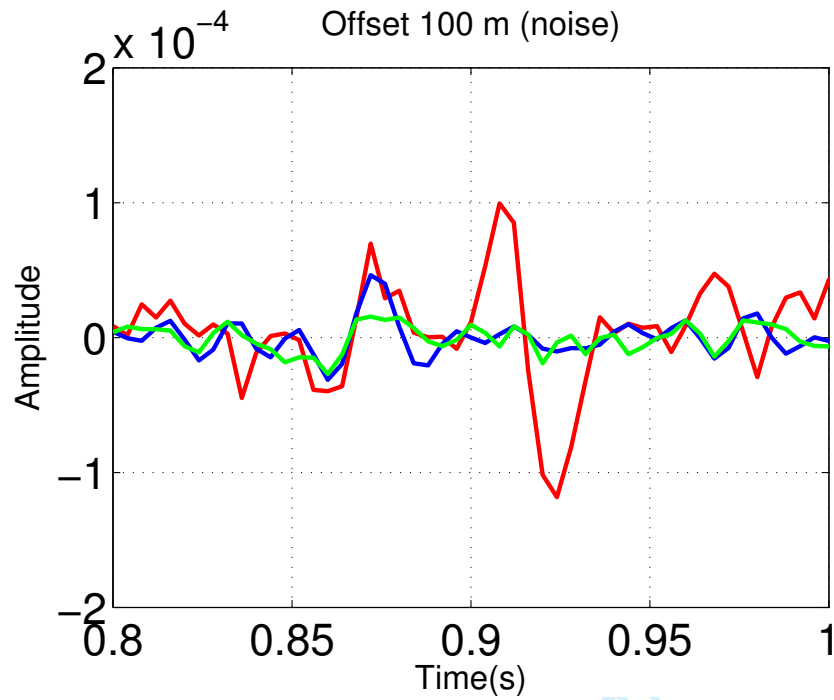


Figure 29: Actual primaries in the data shown in figure 24. –



42 Figure 30: Trace comparison at Offset 100m. Red, blue and green line represent actual
43 data, ISS free-surface multiple prediction and SRME prediction, respectively.
44
45
46
47
48
49
50
51
52
53
54
55
56
57
58
59
60

1
2
3
4
5
6
7
8
9
10
11
12
13
14
15
16
17
18
19
20
21
22
23
24
25
26
27
28
29
30
31
32
33
34
35
36
37
38
39
40
41
42
43
44
45
46
47
48
49
50
51
52
53
54
55
56
57
58
59
60

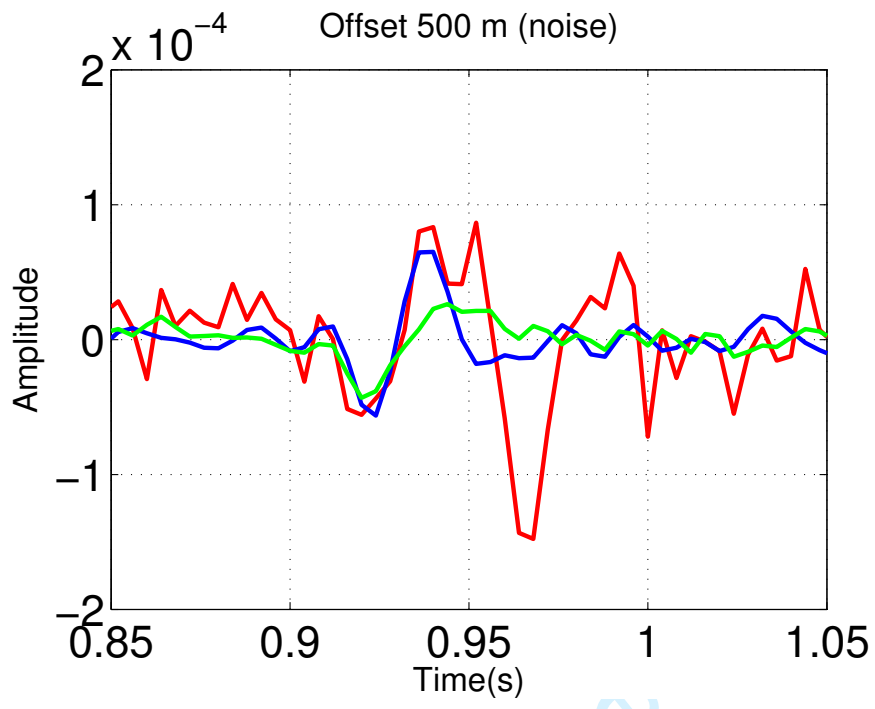


Figure 31: Trace comparison at Offset 500m. Red, blue and green line represent actual data, ISS free-surface multiple prediction and SRME prediction, respectively.

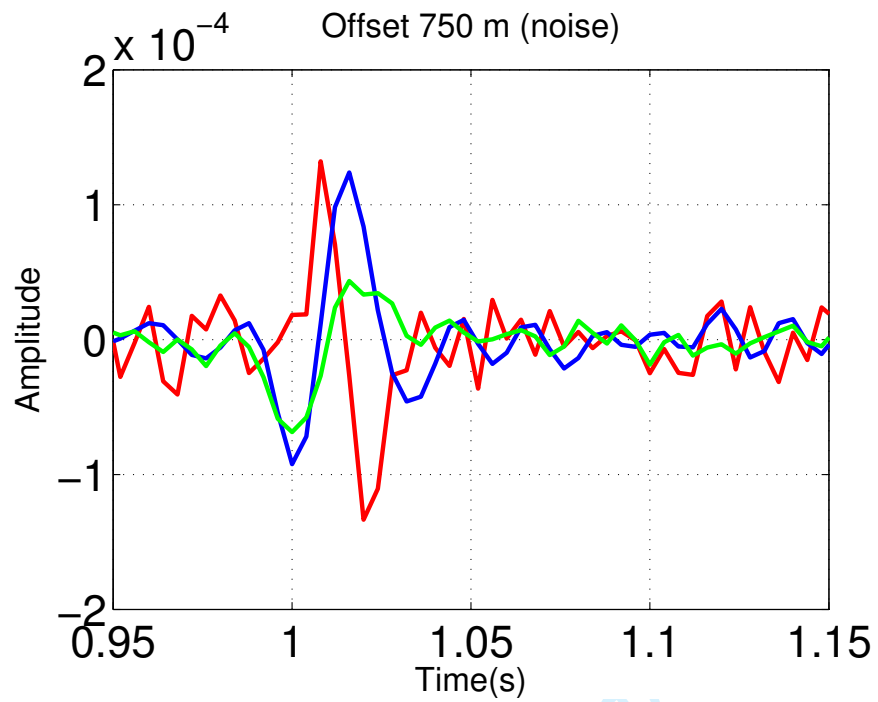


Figure 32: Trace comparison at Offset 750m. Red, blue and green line represent actual data, ISS free-surface multiple prediction and SRME prediction, respectively.

1
2
3
4
5
6
7
8
9
10
11
12
13
14
15
16
17
18
19
20
21
22
23
24
25
26
27
28
29
30
31
32
33
34
35
36
37
38
39
40
41
42
43
44
45
46
47
48
49
50
51
52
53
54
55
56
57
58
59
60

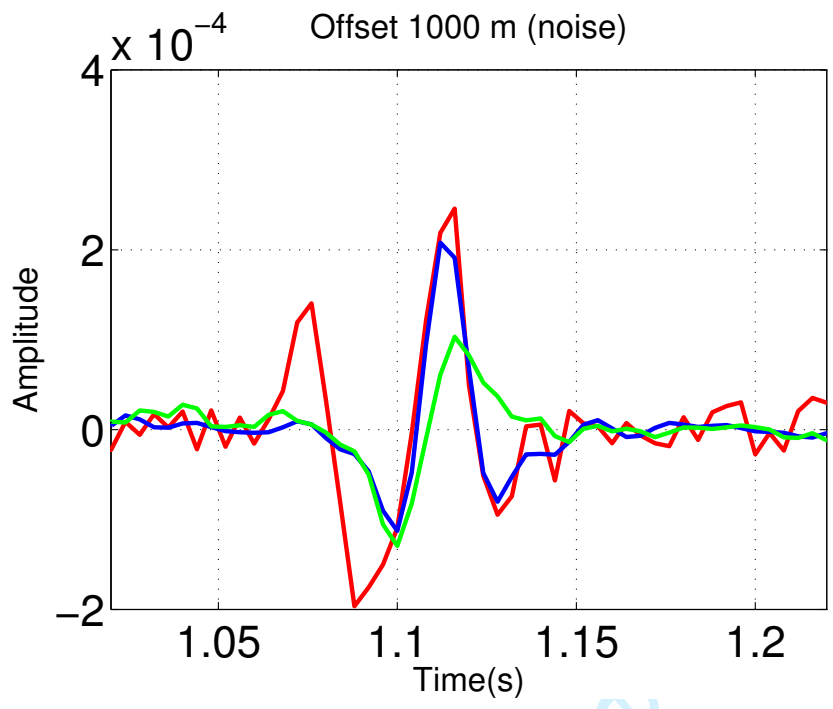
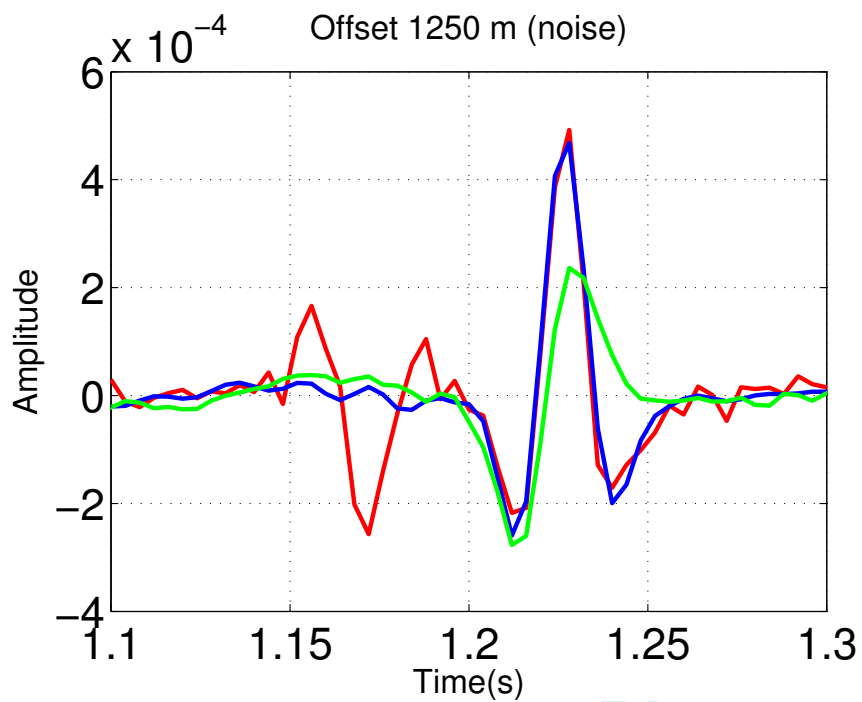


Figure 33: Trace comparison at Offset 1000m. Red, blue and green line represent actual data, ISS free-surface multiple prediction and SRME prediction, respectively.



42 Figure 34: Trace comparison at Offset 1250m. Red, blue and green line represent actual
43 data, ISS free-surface multiple prediction and SRME prediction, respectively.
44
45

1
2
3
4
5
6
7
8
9
10
11
12
13
14
15
16
17
18
19
20
21
22
23
24
25
26
27
28
29
30
31
32
33
34
35
36
37
38
39
40
41
42
43
44
45
46
47
48
49
50
51
52
53
54
55
56
57
58
59
60

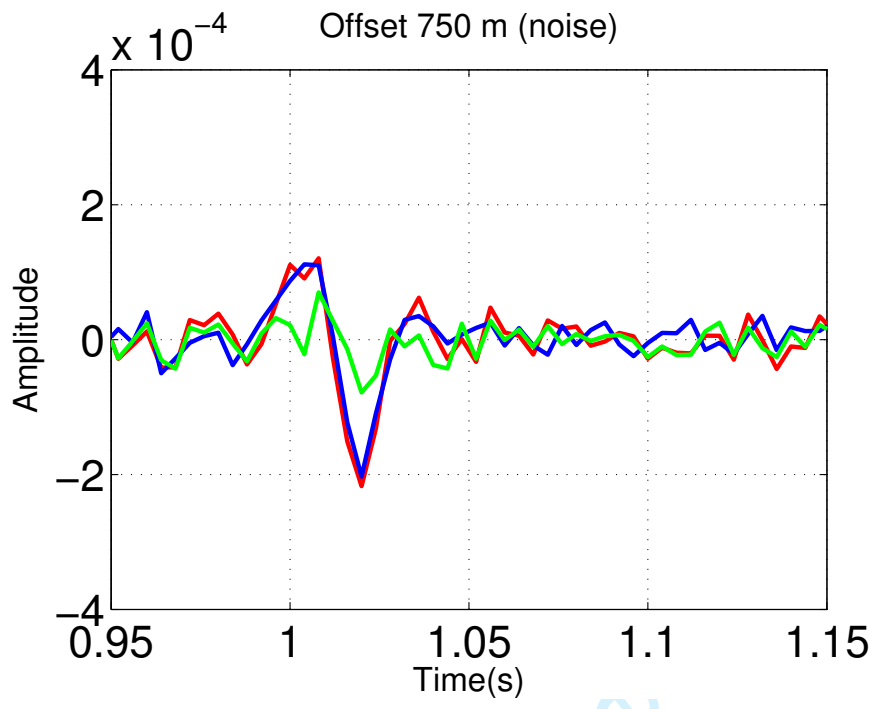


Figure 35: Trace comparison at Offset 750m. Red, blue and green represent the actual primary, result after ISS FSME and result after the SRME + adaptive, respectively.

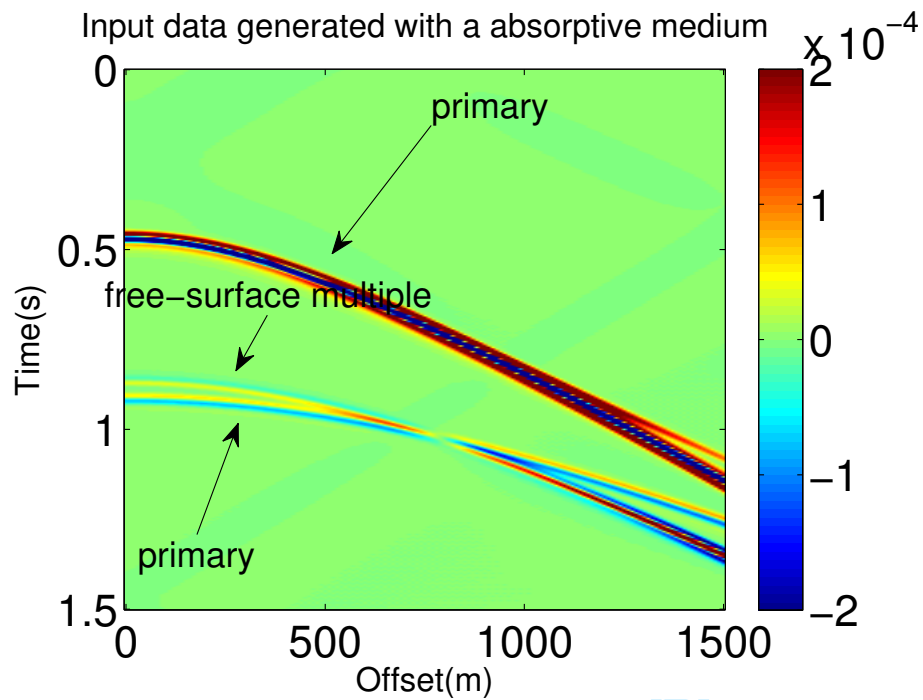


Figure 36: Input data generated from an absorptive medium. –

1
2
3
4
5
6
7
8
9
10
11
12
13
14
15
16
17
18
19
20
21
22
23
24
25
26
27
28
29
30
31
32
33
34
35
36
37
38
39
40
41
42
43
44
45
46
47
48
49
50
51
52
53
54
55
56
57
58
59
60

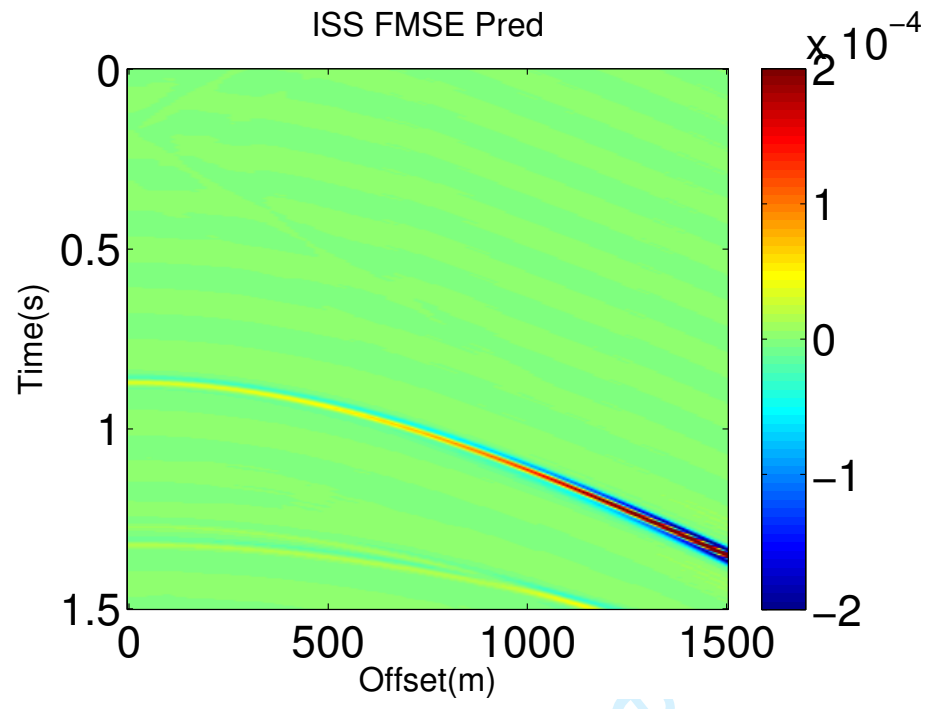
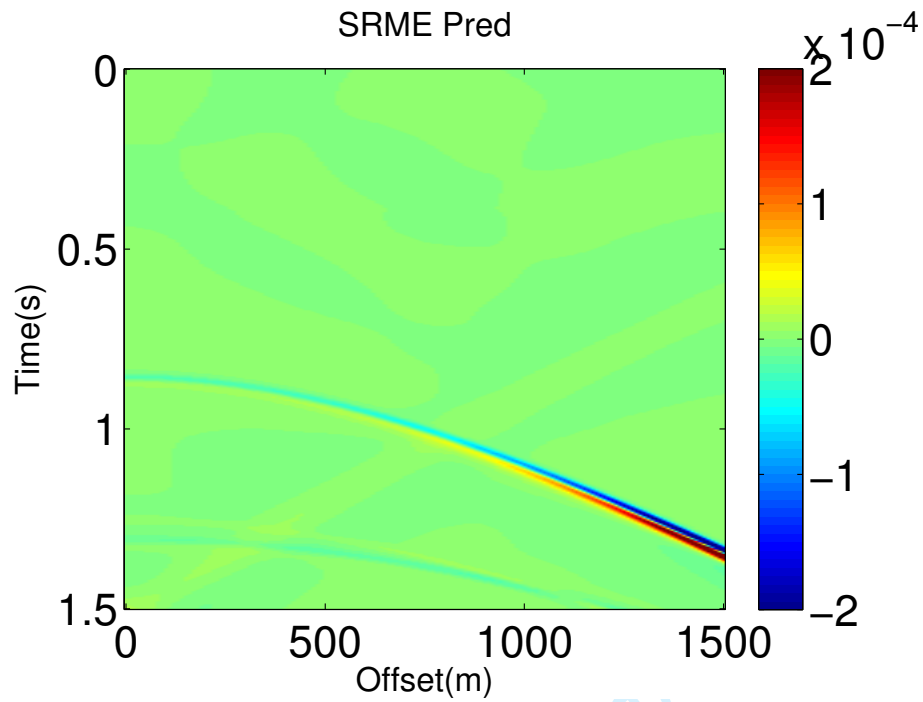


Figure 37: Prediction of free-surface multiple by the ISS FSME (D'_2 in equation 1) using the input data generated by an absorptive medium shown in figure 36.



42 Figure 38: Prediction of free-surface multiple by the SRME using the input data generated
43
44 by an absorptive medium shown in figure 36.
45

46 -

1
2
3
4
5
6
7
8
9
10
11
12
13
14
15
16
17
18
19
20
21
22
23
24
25
26
27
28
29
30
31
32
33
34
35
36
37
38
39
40
41
42
43
44
45
46
47
48
49
50
51
52
53
54
55
56
57
58
59
60

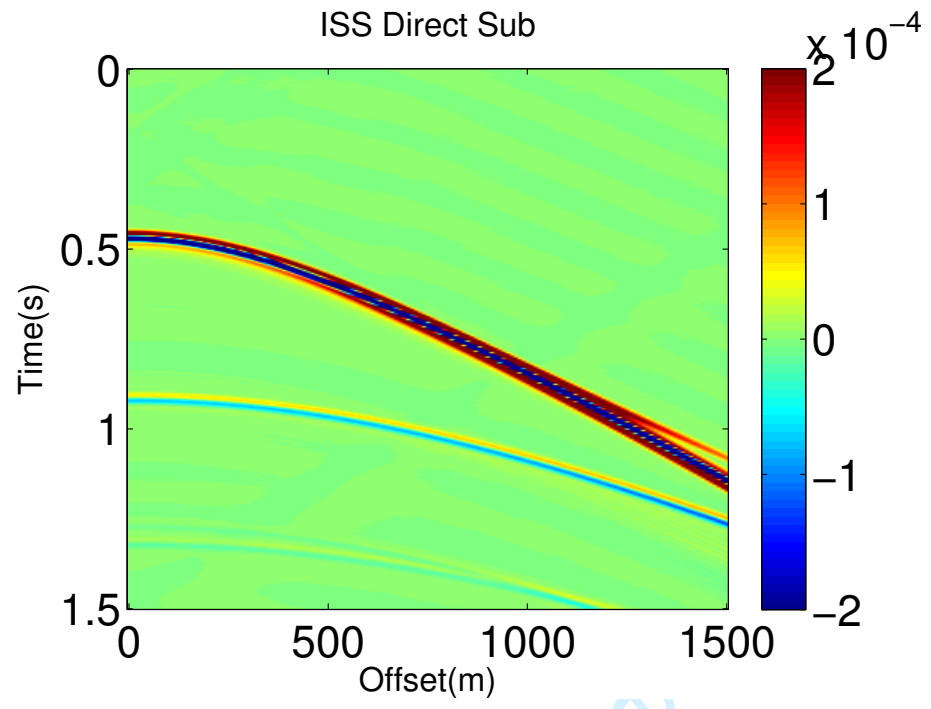
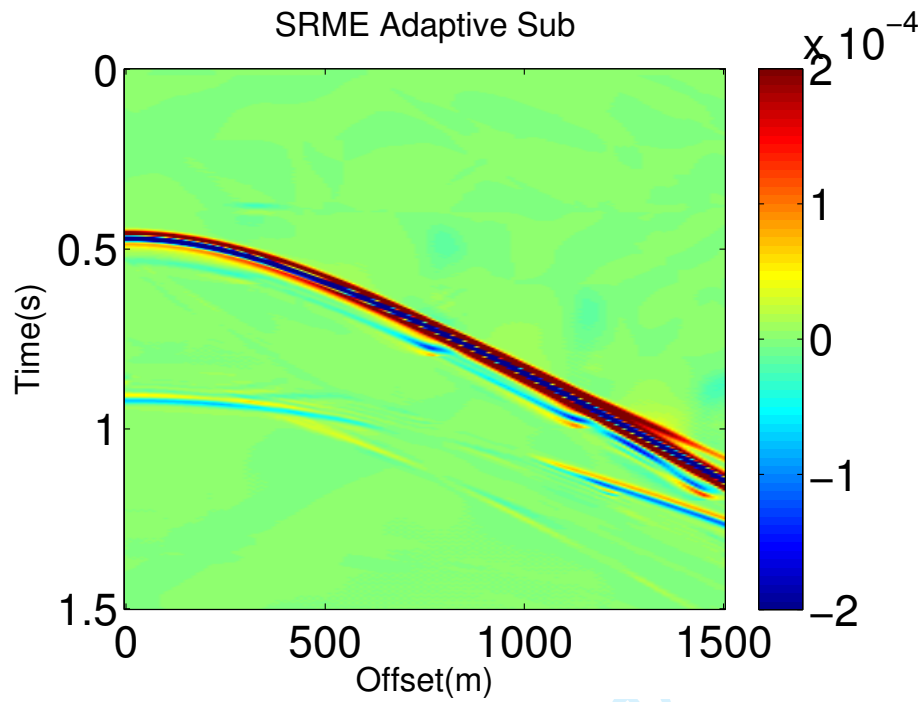


Figure 39: Free-surface multiple removal result after directly subtracting the ISS prediction result (figure 37) from the data (figure 36).



42 Figure 40: Free-surface multiple removal result by combing the SRME prediction (figure
43 38) and adaptive subtraction.
44
45

46 —

1
2
3
4
5
6
7
8
9
10
11
12
13
14
15
16
17
18
19
20
21
22
23
24
25
26
27
28
29
30
31
32
33
34
35
36
37
38
39
40
41
42
43
44
45
46
47
48
49
50
51
52
53
54
55
56
57
58
59
60

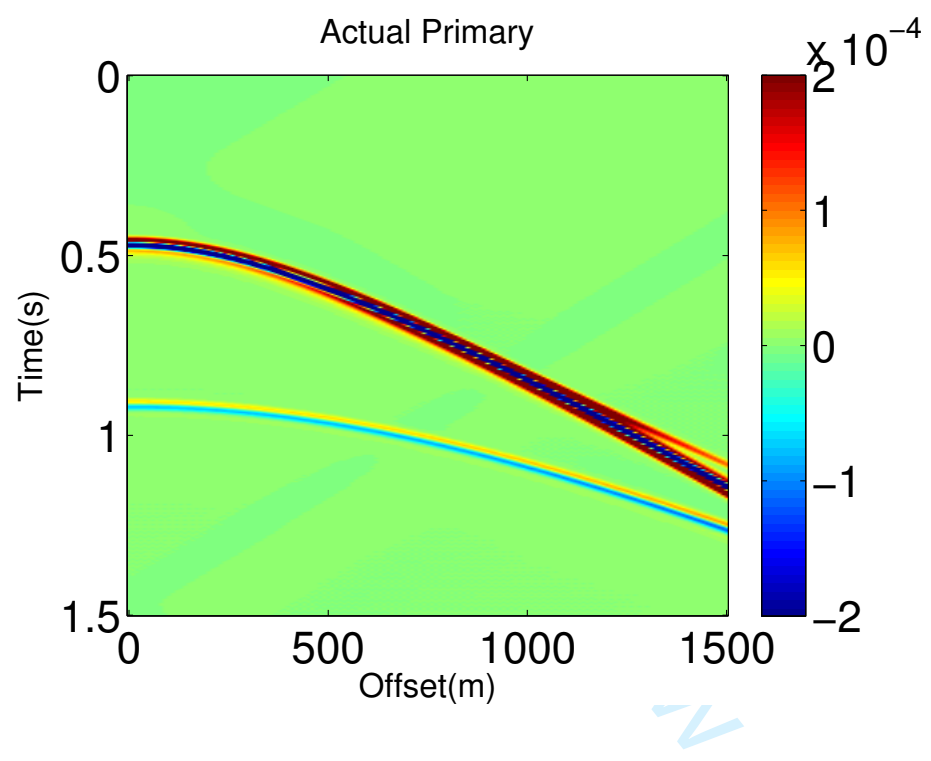
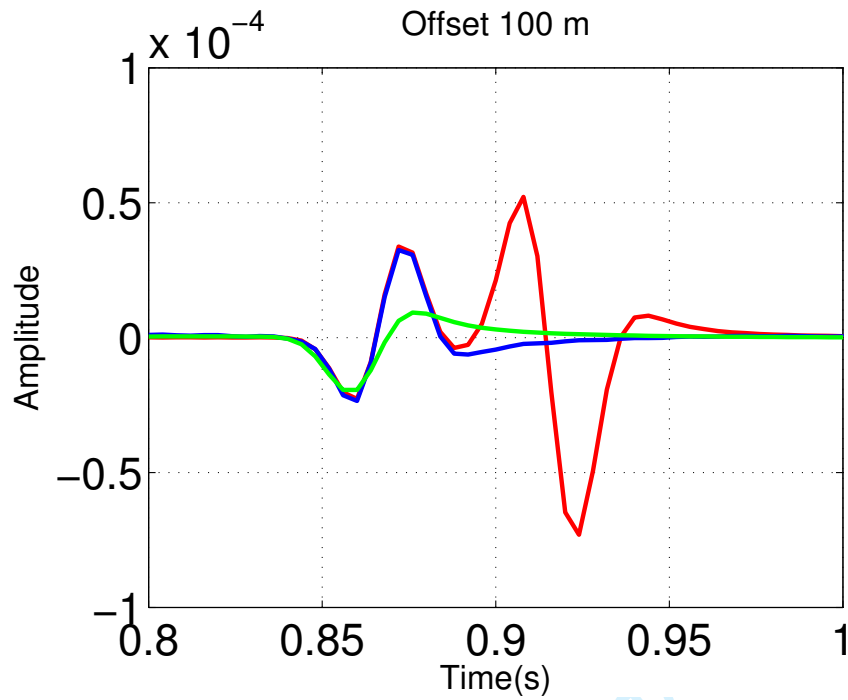


Figure 41: Actual primaries in the input data shown in figure 36. –



42
43
44
45
46
47
48
49
50
51
52
53
54
55
56
57
58
59
60

Figure 42: Trace comparison at Offset 100m. Red, blue and green line represent actual data, ISS free-surface multiple prediction and SRME prediction, respectively.

1
2
3
4
5
6
7
8
9
10
11
12
13
14
15
16
17
18
19
20
21
22
23
24
25
26
27
28
29
30
31
32
33
34
35
36
37
38
39
40
41
42
43
44
45
46
47
48
49
50
51
52
53
54
55
56
57
58
59
60

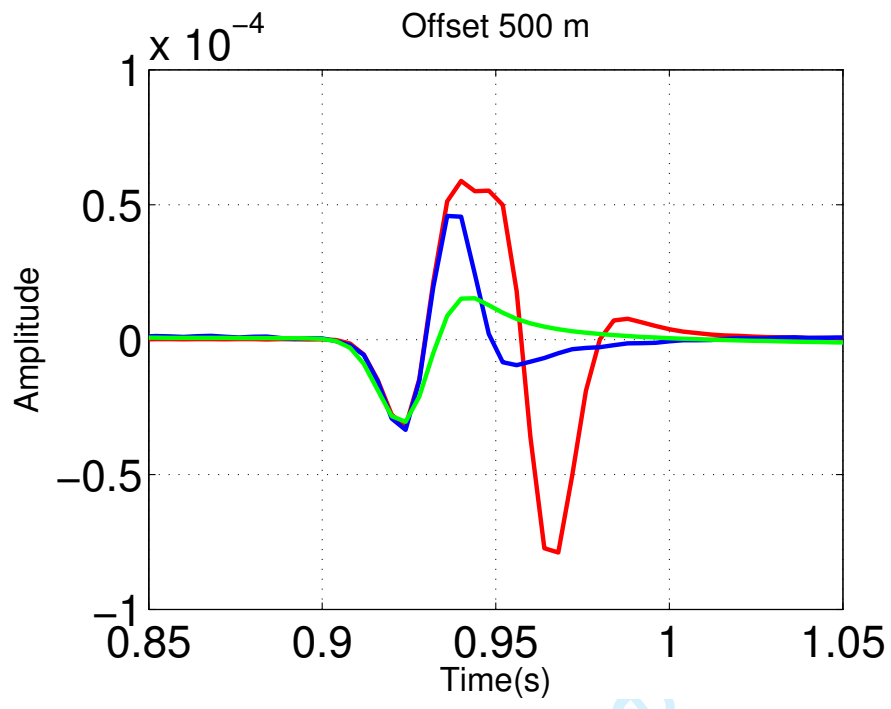


Figure 43: Trace comparison at Offset 500m. Red, blue and green line represent actual data, ISS free-surface multiple prediction and SRME prediction, respectively.

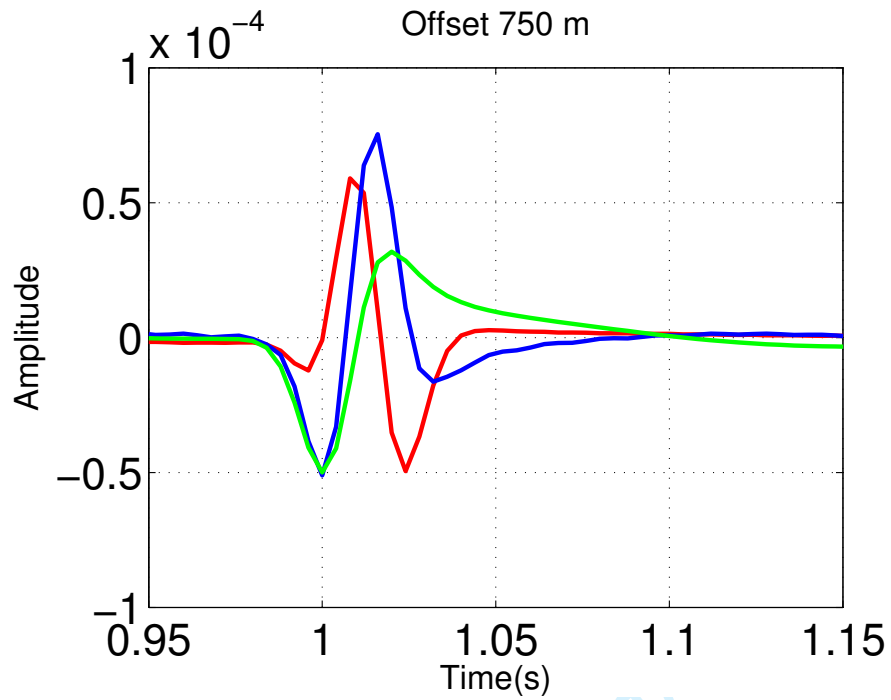


Figure 44: Trace comparison at Offset 750m. Red, blue and green line represent actual data, ISS free-surface multiple prediction and SRME prediction, respectively.

1
2
3
4
5
6
7
8
9
10
11
12
13
14
15
16
17
18
19
20
21
22
23
24
25
26
27
28
29
30
31
32
33
34
35
36
37
38
39
40
41
42
43
44
45
46
47
48
49
50
51
52
53
54
55
56
57
58
59
60

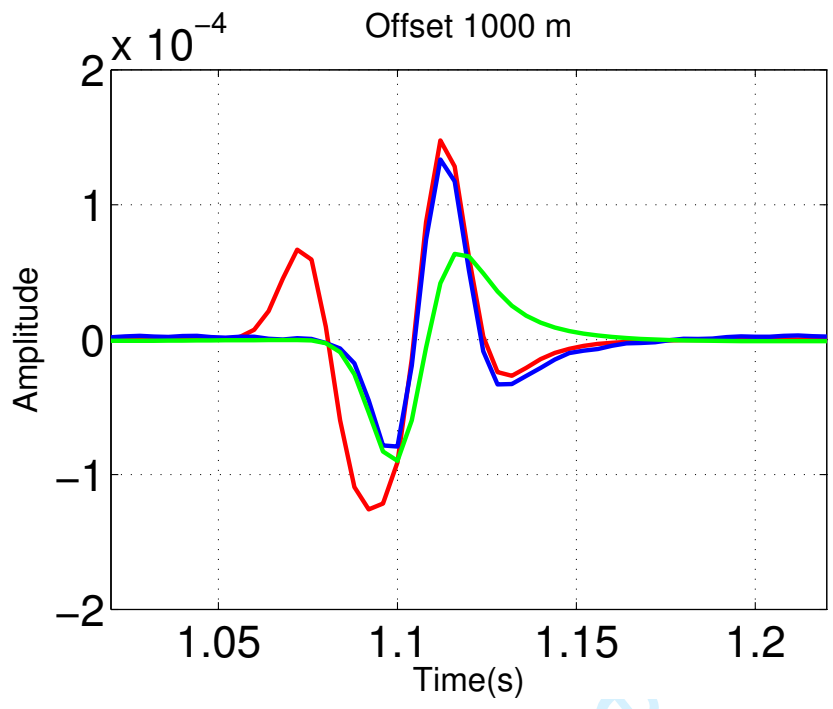


Figure 45: Trace comparison at Offset 1000m. Red, blue and green line represent actual data, ISS free-surface multiple prediction and SRME prediction, respectively.

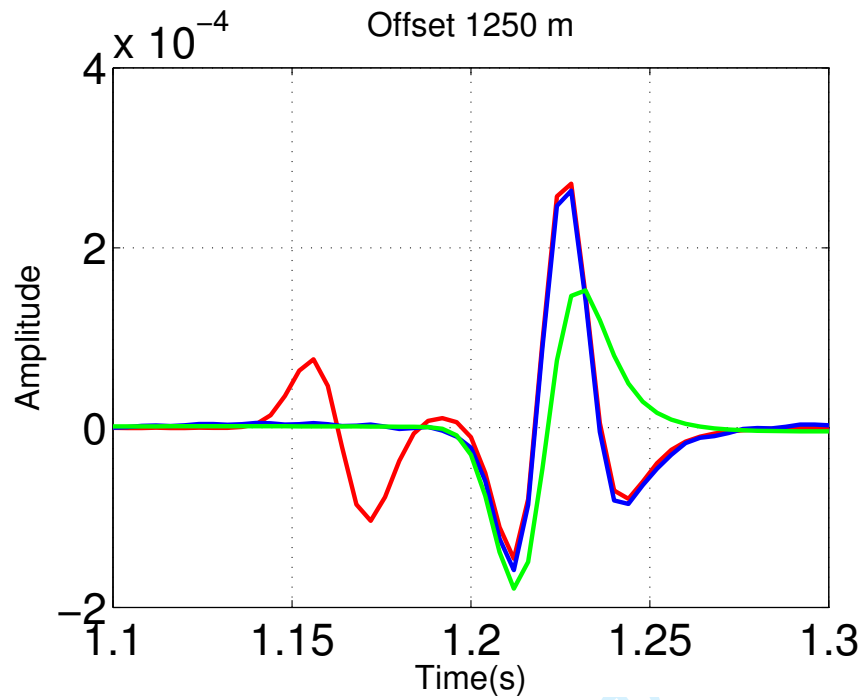


Figure 46: Trace comparison at Offset 1250m. Red, blue and green line represent actual data, ISS free-surface multiple prediction and SRME prediction, respectively.

1
2
3
4
5
6
7
8
9
10
11
12
13
14
15
16
17
18
19
20
21
22
23
24
25
26
27
28
29
30
31
32
33
34
35
36
37
38
39
40
41
42
43
44
45
46
47
48
49
50
51
52
53
54
55
56
57
58
59
60

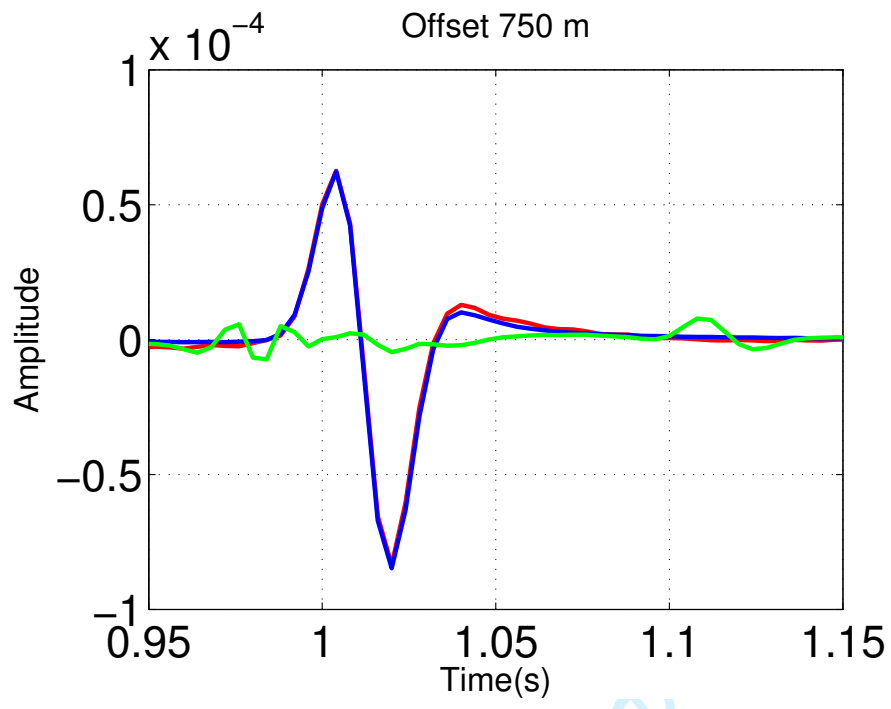
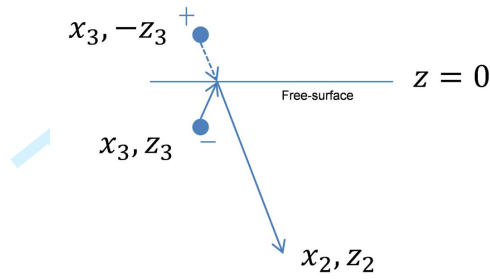


Figure 47: Trace comparison at Offset 750m. Red, blue and green represent the actual primary, result after ISS FSME and result after the SRME + adaptive, respectively.

1
2
3
4
5
6
7
8
9
10
11
12
13
14
15
16
17
18
19
20
21
22
23
24
25
26
27
28
29
30
31
32
33
34
35
36
37
38
39
40
41
42
43
44
45
46
47
48
49
50
51
52
53
54
55
56
57
58
59
60



$$G_0^{fs}(x_2, z_2, x_3, z_3, \omega) = \frac{1}{2\pi} \int dk \frac{e^{ik(x_2-x_3)} e^{iq|z_2-(-z_3)|}}{2iq}$$

$$= \frac{1}{2\pi} \int dk \frac{e^{ik(x_2-x_3)} e^{iq(z_2+z_3)}}{2iq}$$

review

Figure A-1: Green's function G_0^{fs} , travels up from the source to the free-surface and then down to the receiver.

1
2
3
4
5
6
7
8
9
10
11
12
13
14
15
16
17
18
19
20
21
22
23
24
25
26
27
28
29
30
31
32
33
34
35
36
37
38
39
40
41
42
43
44
45
46
47
48
49
50
51
52
53
54
55
56
57
58
59
60

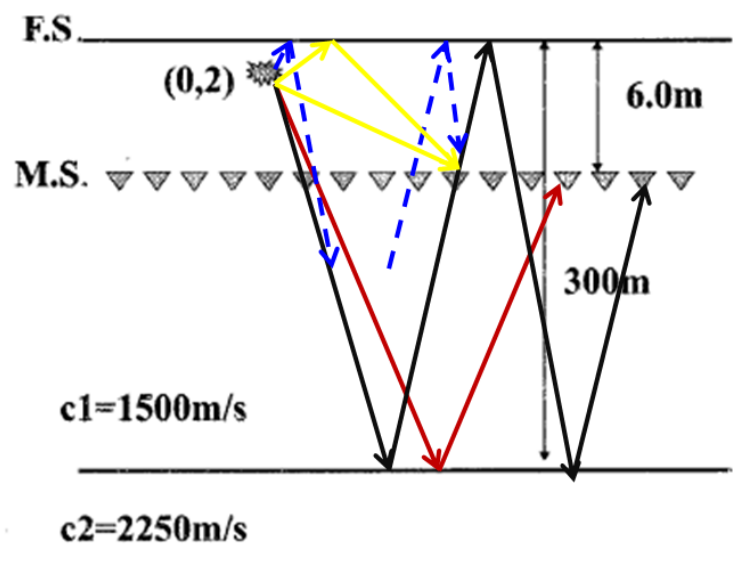


Figure A-2: Model used to generated data in Zhang (2007) to test the ISS FSME. –

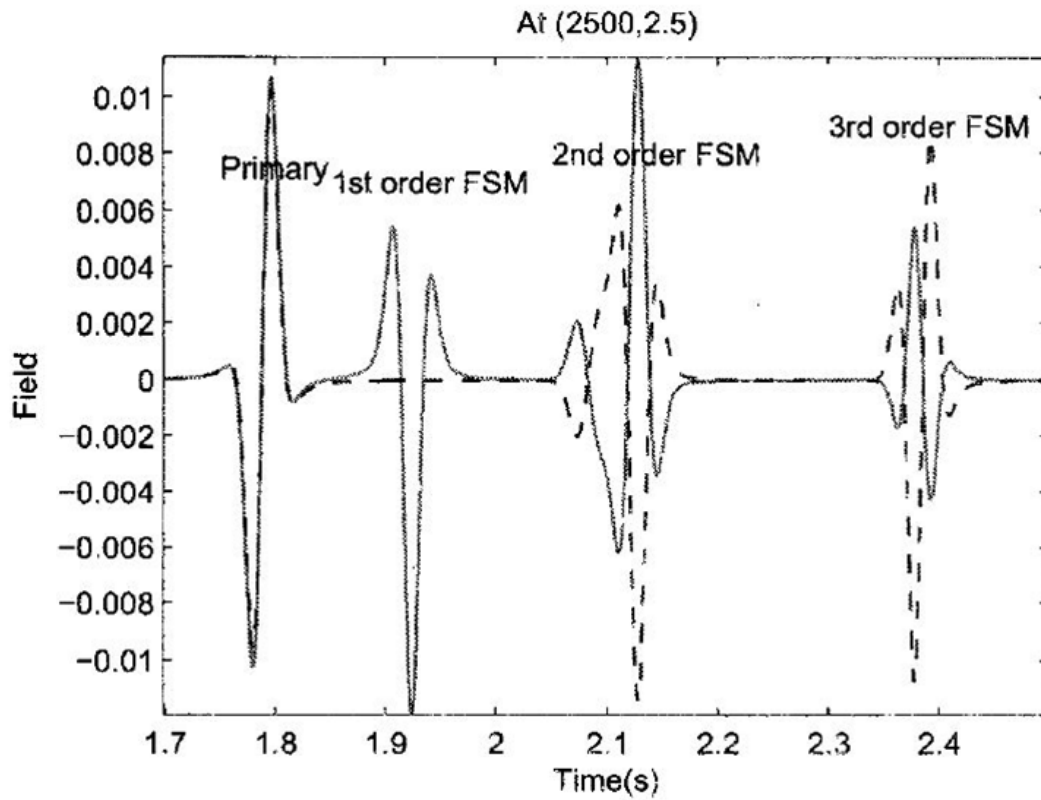


Figure A-3: A trace comparison between the input data D'_1 (solid line) to the ISS FSME and output data $D'_1 + D'_2$ after the ISS FSME. When D'_2 is added to D'_1 , two things happen, the first-order free-surface multiple is eliminated, all higher-order free-surface multiples are altered, and prepared for their removal by D'_3, D'_4 , etc.

1
2
3
4
5
6
7
8
9
10
11
12
13
14
15
16
17
18
19
20
21
22
23
24
25
26
27
28
29
30
31
32
33
34
35
36
37
38
39
40
41
42
43
44
45
46
47
48
49
50
51
52
53
54
55
56
57
58
59
60

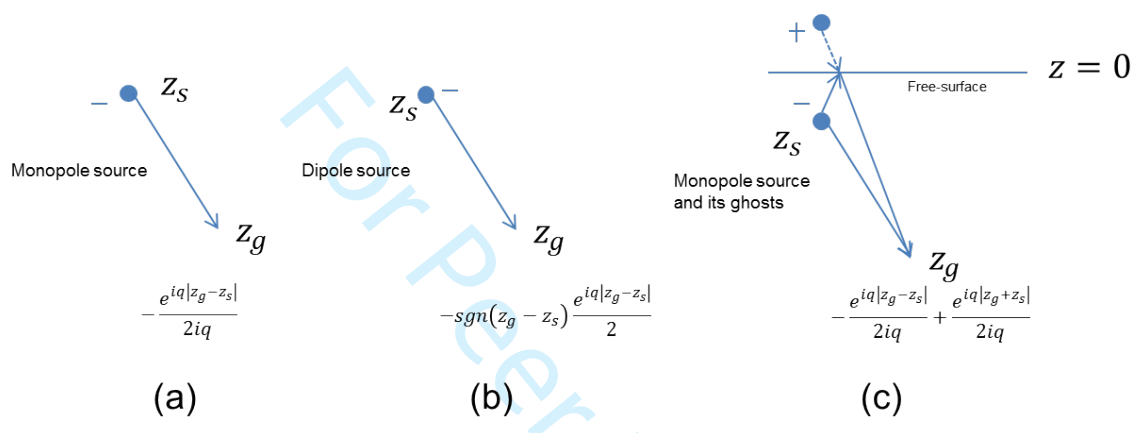


Figure B-1: (a) Monopole source and its 2D Green's function in k_x, ω domain. (b) Dipole source and its 2D Green's function. (c) Monopole source & its source ghosts and their 2D Green's functions. Free-surface is at depth $z = 0$. $q = \sqrt{\frac{\omega^2}{c_0^2} - k_x^2}$, where ω, k_x and c_0 are the temporal frequency, horizontal wavenumber, and medium velocity.